Key Points:
- NO$_3$ uptake, O$_2$:Ar NCP, sediment trap, and ^{234}Th export were measured for 5 months
- New production exceeded export over season-long and region-wide scales
- Vertical mixing of PN to depth may be equal to or greater than sinking flux

Correspondence to:
M. R. Stukel,
mstukel@fsu.edu

The imbalance of new and export production in the western Antarctic Peninsula, a potentially "leaky" ecosystem

Michael R. Stukel[1], Elizabeth Asher[2], Nicole Couto[3], Oscar Schofield[3], Stefanie Strebel[4], Philippe Tortell[2,5], and Hugh W. Ducklow[6]

[1]Department of Earth, Ocean, and Atmospheric Science, Florida State University, Tallahassee, Florida, USA, [2]Department of Earth, Ocean, and Atmospheric Sciences, University of British Columbia, Vancouver, British Columbia, Canada, [3]Department of Marine and Coastal Sciences, Rutgers University, New Brunswick, New Jersey, USA, [4]Marine Biological Laboratory, Woods Hole, Massachusetts, USA, [5]Department of Botany, University of British Columbia, Vancouver, British Columbia, Canada, [6]Lamont-Doherty Earth Observatory, Columbia University, Palisades, New York, USA

Abstract To quantify the balance between new production and vertical nitrogen export of sinking particles, we measured nitrate uptake, net nitrate drawdown, ΔO_2/Ar-based net community production, sediment trap flux, and ^{234}Th export at a coastal site near Palmer Station, Antarctica, during the phytoplankton growing season from October 2012 to March 2013. We also measured nitrate uptake and ^{234}Th export throughout the northern western Antarctic Peninsula (WAP) region on a cruise in January 2013. We used a nonsteady state ^{234}Th equation with temporally varying upwelling rates and an irradiance-based phytoplankton production model to correct our export and new production estimates in the complex coastal site near Palmer Station. Results unequivocally showed that nitrate uptake and net community production were significantly greater than the sinking particle export on region-wide spatial scales and season-long temporal scales. At our coastal site, new production (105 ± 17.4 mg N m^{-2} d^{-1}, mean ± standard error) was 5.3 times greater than vertical nitrogen export (20.4 ± 2.4 mg N m^{-2} d^{-1}). On the January cruise in the northern WAP, new production (47.9 ± 14.4 mg N m^{-2} d^{-1}) was 2.4 times greater than export (19.9 ± 1.4 mg N m^{-2} d^{-1}). Much of this imbalance can be attributed to diffusive losses of particulate nitrogen from the surface ocean due to diapycnal mixing, indicative of a "leaky" WAP ecosystem. If these diffusive losses are common in other systems where new production exceeds export, it may be necessary to revise current estimates of the ocean's biological pump.

1. Introduction

The balance of new and export production has been a structuring principle in marine biogeochemistry since the seminal work of *Eppley and Peterson* [1979]. When integrated over sufficiently large spatial and long temporal scales, mass balance requires that new production (primary production supported by exogenous sources of N, primarily upwelled NO$_3^-$ in polar regions) be balanced by N losses. However, the assumption that total export is dominated by the vertical flux of sinking particles into the ocean's interior does not necessarily follow. Paired measurements of new production and particle export are relatively uncommon and suffer from methodological issues associated with sediment traps [*Baker et al.*, 1988; *Buesseler et al.*, 2007], which have historically been the most commonly used method for quantifying vertical flux. The imbalance that is typically measured in these studies is often ascribed to temporal or spatial decoupling of new and export production, or to hydrodynamic biases of the deployed traps [*Baker et al.*, 1988; *Buesseler et al.*, 2007]. The difficulty of undertaking long-term studies across large regions with multiple complementary methods has thus far prevented investigators from testing rigorously the fundamental assumption of balanced new and export production that shapes our understanding of carbon and nitrogen cycles.

Continental margins play a disproportionately important role in C and N fluxes [*Hedges*, 1992; *Ducklow and McCallister*, 2004], yet these fluxes are difficult to assess due to large temporal variability, sharp spatial gradients, and complex flow regimes. High-latitude continental margins exhibit particularly strong seasonal cycles, which interact with interannual variations and longer-term forcing. The biogeochemical state of coastal and shelf regions of Antarctica remains particularly poorly understood due to remote location and sampling difficulties imposed by sea ice [*Ducklow et al.*, 2007]. The marine ecosystem of the western Antarctic Peninsula (WAP) extends for 1300 km along the coast and from a rocky, glaciated shore across the continental shelf and
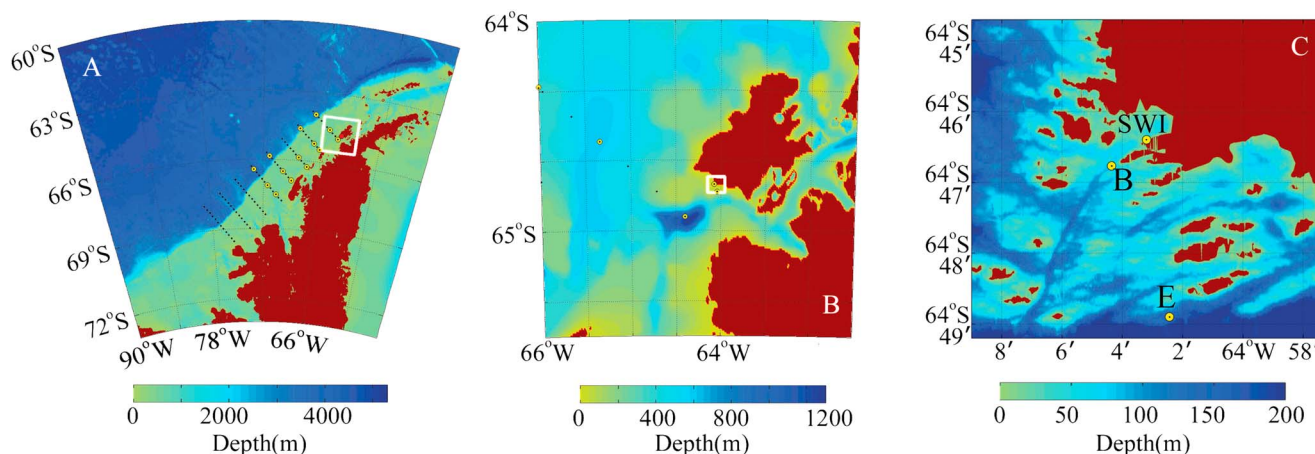
Figure 1. (a) The bathymetry of our study region within the broader context of the western Antarctic Peninsula. The black points are offshore stations sampled on the January cruises. The yellow bulls-eyes are the stations sampled for [234]Th on the January 2012 LTER cruise. The white box shows the Anvers Island region, which is shown in greater detail in (b). (c) Our primary sampling location at Station E as well as our ancillary sampling site (Station B) and the seawater intake for Palmer Station (SWI). The white box in Figure 1b shows the Palmer Station region, which is highlighted in Figure 1c. Note the different color axes used for depth in each plot.

into deep water (Figure 1). This heterogeneous region is one of the fastest warming areas on Earth, with a 7°C winter temperature increase since 1950 [*Ducklow et al.*, 2013], that has been accompanied by latitudinally variable changes in phytoplankton concentrations [*Montes-Hugo et al.*, 2009]. The WAP ecosystem is characterized by high surface nitrate concentrations, strong seasonal diatom blooms, and a dominant role for large krill and salps [*Ducklow et al.*, 2007; *Steinberg et al.*, 2012; *Ducklow et al.*, 2013]—all of which would typically point to an efficient biological pump [*Michaels and Silver*, 1988; *Ducklow et al.*, 2001]. Indeed, high net community production (NCP) has been measured throughout the WAP using geochemical tracers [*Huang et al.*, 2010]. However, a multidecade time series of moored sediment traps on the continental shelf in the WAP has measured relatively low rates of particle export [*Ducklow et al.*, 2008]. [234]Th results have suggested that the moored trap may be undercollecting by a factor of 20 [*Buesseler et al.*, 2010], calling into question the use of these traps as a quantitative measure of carbon flux.

Since the initial *Eppley and Peterson* [1979] hypothesis about the balance between new and export production, new techniques have become available for assessing these quantities. O_2:Ar ratios can be used to determine net community production (NCP, which should be functionally similar to new production) because O_2 and Ar behave similarly with respect to air-sea transfer properties [*Craig and Hayward*, 1987; *Reuer et al.*, 2007]. Thus, changes in the ratio must be due to net biological production or utilization of O_2. [234]Th:[238]U disequilibrium can be used to measure particle export since [238]U remains dissolved in the surface ocean, while its first long-lived daughter particle, [234]Th (half-life 24 days), is removed from the upper water column by adsorption onto sinking particles [*Waples et al.*, 2006]. By combining these newer measurement techniques with traditional measurement tools ([15]NO_3^- uptake, net nitrate drawdown, sediment traps) during a five monthlong austral summer season at Palmer Station in the WAP, we have been able to follow seasonal patterns of new and export production. Additional region-wide sampling in January 2013 enabled us to extrapolate our measurements across a broader spatial area.

2. Methods

2.1. Oceanographic Sampling Near Palmer Station

Temperature, salinity, and chlorophyll *a* (Chl *a*) fluorescence were determined twice weekly with a SBE 19+ Seabird conductivity-temperature-depth (CTD) at two sampling sites (Stations B and E; Figure 1) near Palmer Station (64.815°S, 64.041°W) from late October 2012 until early April 2013. Chlorophyll *a* was measured at seven depths from the surface to 65 m using the fluorometric method with an acidification step to account for phaeo-pigments [*Strickland and Parsons*, 1972]. Particulate organic carbon and nitrogen (POC, PN) samples were collected at the same depths as Chl *a* at Station E and filtered onto precombusted GF/F filters prior to analysis on a CHN analyzer. [14]C primary production (24 h incubations) was measured twice weekly at 5 fixed depths

(0, 5, 10, 20, and 65 m) following established Palmer Long Term Ecological Research (LTER) protocols [*Smith et al.*, 2001]. Light spectral characteristics and photosynthetically active radiation (PAR) were measured from late October through early January using a Satlantic HyperOCR hyperspectral radiometer attached to a free-falling MicroPro Ocean Profiler and surface light meter. O_2:Ar ratios were also measured continuously from the near-shore seawater intake at Palmer Station using a membrane inlet mass spectrometer. Changes in this ratio are indicative of the net balance between respiration and photosynthesis, because Ar behaves similarly to O_2 with respect to physical changes in saturation state, but is not utilized by plankton. We thus used a mass balance approach to estimate NCP from temporal deviations in O_2:Ar (see *Tortell et al.* [2014] for additional details).

2.2. Sediment Trap

We used a moored version of Vertical Transport and Exchange Study-style sediment traps to estimate particle export from the upper 50 m. The trap array consisted of four acrylic particle-interceptor trap (PIT) tubes (60-cm height, 7-cm internal diameter) with a baffle composed of 13 smaller tubes with tapered ends, on a PVC cross-piece [*Knauer et al.*, 1979; *Stukel et al.*, 2013]. The trap was located at 50 m depth in ~170 m deep water near Station E during the ice-free season or at 50 m depth in ~80 m deep water at Station B at the beginning and end of the season when ice conditions did not allow deployment at Station E. The trap array included a surface float line above the trap, a 12 kg chain immediately below the trap, and a 22 kg anchor. Prior to deployment, PIT tubes were filled with 2.0 L of a saltwater slurry made from 0.1 μm Acro-pak filtered seawater amended with an additional 40 g L^{-1} NaCl and borate-buffered formaldehyde (final concentration 0.4%). Trap deployments during the middle of the season were of roughly 1 week duration, with the trap redeployed immediately following recovery. At the beginning and end of the season, when brash ice increased the risk of losing the trap, deployments were shortened to a period of 2–4 days and the trap array was removed from the water between deployments.

After recovery, overlying lower density water that had been mixed into the PIT tubes was immediately removed by gentle suction on the zodiac sampling platform. In the laboratory, the remaining material was filtered through a 200 μm mesh. The filtrate was filtered through a precombusted quartz (QMA) filter, which was then beta counted (see below) to determine ^{234}Th concentration prior to combustion for C and N. The material on the 200 μm filter was inspected under a Leica MZ 7.5 stereomicroscope to allow removal of mesozooplankton swimmers. The remainder of the >200 μm sample was then washed off the 200 μm mesh and filtered through a precombusted QMA filter for C:N:^{234}Th analyses of the large size-fraction of sinking material.

2.3. Water Column ^{234}Th Sampling

Samples were collected approximately weekly at Station E to characterize ^{234}Th distributions in the water column. 3–4 liter samples (exact volume determined gravimetrically on land) for total ^{234}Th were collected in Go-Flo bottles from eight depths (0, 5, 10, 20, 35, 50, 65, and 100 m). After returning to Palmer Station, samples were weighed and acidified to a pH of <2 with HNO_3. A tracer addition of ^{230}Th (either 0.5 or 1.0 mL of 4.6 pCi mL^{-1} ^{230}Th) was immediately added, and samples were mixed vigorously. Typically, 2–3 h passed between sample collection and acidification in the laboratory. Samples were allowed to equilibrate for 4–9 h, and the pH was then raised to 8–9 with NH_4OH addition. One hundred microliters each of $KMnO_4$ (7.5 g L^{-1}) and $MnCl_2$ (33 g L^{-1}) were added, and samples were mixed and allowed to sit for ~12 h as Th coprecipitated with manganese oxide. Samples were then vacuum filtered at high vacuum onto QMA filters, dried at 50°C, and mounted in RISO sample holders. Samples were counted on a low-level beta GM multi-counter (DTU RISØ National Laboratory, Roskilde, Denmark) at Palmer Station for a period of 12 to 24 h to determine initial radioactivity (detector efficiencies, calculated separately for each position, varied from 0.39 to 0.41). After >6 half-lives, they were again counted on the beta counter to determine background beta emissions. Samples were then dissolved in 8 M HNO_3/10% H_2O_2, spiked with a gravimetric addition of ^{229}Th, and sonicated for 20 min. They were then sent to the Woods Hole Oceanographic Institution Analytical Facility (Woods Hole, MA) for inductively coupled plasma–mass spectrometric analysis of the $^{229:230}$Th ratio [*Benitez-Nelson et al.*, 2001; *Pike et al.*, 2005]. Average yield was 90.6% for samples collected at Palmer Station and 90.2% for samples collected on the January cruise.

2.4. ^{15}NO$_3$ Uptake

Samples were collected in Go-Flo bottles from five depths at Station E (0, 5, 10, 20, and 65 m) and immediately transferred gently with silicon tubing into 1.2 L polycarbonate bottles shaded at light levels of 100%, 50%,

25%, 10%, and 0% surface irradiance (as for the ^{14}C primary production measurements). Screening was representative of in situ light levels through most of the season, but during the height of the bloom (late November to early December) light levels experienced in situ were likely significantly less at 5–20 m than those experienced within the bottles. Upon return to Palmer Station, samples were spiked with ^{15}NO$_3^-$ to a final concentration of 1 μM ^{15}NO$_3^-$ early in the season or 0.5 μM ^{15}NO$_3^-$ later in the season when NO$_3^-$ concentrations were presumed to have decreased. Samples were then incubated for 24 h in outdoor flow-through incubators. After incubation, samples were filtered through precombusted GF/F filters and frozen at −80°C. Samples were analyzed on a mass spectrometer at the University of California, Davis Analytical Facility [*Dugdale and Wilkerson*, 1986].

2.5. Spatiotemporal Interpolation

To smooth and interpolate our unevenly sampled data fields from Station E, we began by computing two-dimensional (depth-time) empirical semivariograms (a semivariogram is a plot of the spatiotemporal autocorrelation between sampling points). Since the distinct temporal patterns of the Antarctic growth season (bloom in November–December, lower biomass before and after) combined with our ~5 months of measurements would lead to a peak in the semivariogram at intermediate time differentials, we truncated the empirical semivariogram at a time differential of 1 month. Anisotropic semivariogram models were then calculated with a spherical model (using equivalent isotropic lag to account for different ranges in time and depth) and a nugget defined to be equal to the mean squared measurement uncertainty for the respective data field. We then used ordinary kriging techniques [*Krige*, 1951; *Isaaks and Sarivasta*, 1989; *Stein*, 1999] to compute gridded (1 day × 1 m) property estimates and uncertainties for water column ^{234}Th concentration, NO$_3^-$, PN, Chl a, CTD fluorescence, density, and light attenuation coefficient.

2.6. Primary Production and Nitrate Uptake Model

For practical reasons, sampled depths were incubated at fixed light levels for both H^{14}CO$_3^-$ and ^{15}NO$_3^-$ uptake throughout the season despite substantial variability in the depth of the euphotic zone. To account for the change in light level, as well as daily variability in surface irradiance, we modeled primary production based on the *Moline et al.*'s [1998] equation: PP = P_{max} × Chl × tanh(PAR/I_k). We determined P_{max} and I_k from our H^{14}CO$_3^-$ uptake incubations, combined with contemporaneous Chl a measurements and PAR determined by multiplying 24 h averages of Palmer Station surface PAR by our incubation light percentages (we assumed that "dark" bottles were actually incubated at ~1% light level). Under the assumption that the phytoplankton community composition evolved in time throughout the season, we computed I_k and P_{max} with a 2 week exponential moving average and used Monte Carlo error analysis to determine uncertainty for these parameters. To model nitrate uptake, we first computed empirical f ratios from paired ^{15}NO$_3^-$ uptake and ^{14}C-PP measurements (f = Up$_{NO3}$/Up$_{HCO3}$ × 6.625 molC:molN, truncated to a maximum f ratio of 1). We found no relationship between f ratio and either depth or nitrate concentration, likely because phytoplankton were not nitrate-limited. We therefore assumed that the f ratio was determined primarily by protistan community dynamics and hence calculated a temporally varying model f ratio as a production-weighted 2 week exponential moving average derived from our measurements. The modeled f ratio was then multiplied by our modeled primary production to model nitrate uptake.

To determine light levels for November and December, we utilized light absorption coefficients calculated over 5 m bins with the in situ hyperspectral radiometer. Because these data were not available for January through March, we computed a Type II (geometric mean) regression of light absorption coefficient on Chl a fluorescence: Abs = 0.050 (±0.003) + 0.036 (±0.002) × Fluor (N = 397, r^2 = 0.185). Relative in situ light levels (% surface irradiance) were calculated by integrating the downward light absorption using the gridded absorption coefficient field. These relative values were multiplied by surface irradiance levels (measured continuously from the Palmer Station weather sensors) to determine in situ PAR throughout the season. Gridded chlorophyll estimates (created using kriging techniques as explained above) were then combined with in situ light levels and the temporally varying P_{max}, I_k, and f ratio values for the community to estimate primary and new production.

2.7. Uncertainty Analysis

To determine the uncertainty in derived parameters (e.g., ^{234}Th export and nitrate uptake), we began with the gridded uncertainties in each measured standing stock as determined by kriging statistical analyses (above). We then followed standard propagation of error rules to determine uncertainty in derived parameters. For

example, to determine ^{234}Th export with a nonsteady state (without upwelling) model, we began by determining uncertainty in vertically integrated ^{234}Th for the surface 50 m:

$$\sigma_{VI234Th} = \sqrt{\sum_{depth=0}^{50} \sigma_{234Th}^2}$$

(1)

where $\sigma_{VI234Th}$ is the uncertainty in vertically integrated ^{234}Th and σ_{234Th} is the kriging-derived uncertainty in ^{234}Th at any specific depth. We then independently computed the uncertainty for the steady state (SS) and nonsteady state (NSS) terms of the ^{234}Th budget (for more details on these terms see our results section (equations (5)–(10)):

$$\sigma_{SS} = \lambda \sqrt{\sigma_{VI234Th}^2 + \sigma_{VI238U}^2}$$

(2)

where σ_{VI238U} is the vertically integrated uncertainty in ^{238}U (determined from the relationship in *Owens et al.* [2011]) and σ_{NSS} is derived from the uncertainty in rates of change of vertically integrated ^{234}Th. Note that σ_{NSS} is inversely related to the time span being considered, and hence, the NSS term has high uncertainty when determining the amount of export over a 1 day or few day periods, but considerably less uncertainty when determining the amount of export for a 2 week period (and adds almost no uncertainty to the total ^{234}Th budget when determining the amount of export occurring over a seasonal time scale). Note that since we have used the kriging method (which determines a linear unbiased prediction of ^{234}Th values) to interpolate ^{234}Th measurements from multiple profiles we chose to use the approach of *Buesseler et al.* [2005] rather than the alternative approach of calculating a single SS + NSS term (equations (4) and (5) of *Savoye et al.* [2006]), which would be more appropriate if determining average export between two sampling points. We then determine the full uncertainty of the nonsteady state (without upwelling) ^{234}Th equation as

$$\sigma_{export} = \sqrt{\sigma_{SS}^2 + \sigma_{NSS}^2}$$

(3)

(note that when considering a longer time period than a day, the uncertainty must be propagated through several different days of σ_{SS}).

Calculation of parameters for modeled primary production and nitrate uptake (P_{max}, I_k, and f) used measurements collected from multiple sampling points. Therefore, derived values for any one of these parameters are highly correlated on short time scales. Since the covariance term in typical propagation of error measurements can thus not be assumed to be zero (and cannot simply be calculated as it varies significantly based on the spatiotemporal density of sampling points), we used a Monte Carlo approach (sampling with replacement) to determine uncertainty estimates associated with modeled primary production and nitrate uptake. Unless otherwise stated, all uncertainty estimates given in this manuscript are ±standard error (thus giving our uncertainty in the mean of the estimate).

2.8. Ship-Based Estimates of Regional Nitrate Uptake and ^{234}Th Export

On the January 2013 Palmer LTER cruise aboard ARSV Laurence M Gould, we collected samples for ^{234}Th (typically eight depths per profile in addition to a 2000 m sample taken, when possible, for calibration), ^{14}C primary production (typically five depths), and NO_3^- uptake (typically three depths, ~100%, 33%, and 10% surface irradiation) at 13 stations along the WAP (Figure 1) using methods described above. ^{234}Th export was calculated using a one-dimensional steady state equation [*Savoye et al.*, 2006] and vertically integrated to the depth of the deepest primary productivity sample (nominally 0.5% light level, average 56 m). ^{234}Th fluxes were converted to N fluxes by multiplying by the N:^{234}Th ratio of particles collected in 50 m sediment traps at Station E . In principle, this approach may lead to a slight bias in N flux since the N:^{234}Th ratio can vary (particularly with depth). In practice, however, we found that the sinking flux near Palmer Station showed little seasonal variation in the N:^{234}Th ratio despite large changes in community composition and particulate standing stock. Since we were limited to three NO_3^- incubation depths, we computed an equivalent vertically integrated f ratio by comparing paired NO_3^- uptake and primary production experiments and multiplying this f ratio by the full water column integrated primary production to estimate vertically integrated NO_3^- uptake. This approach may yield slight underestimates if higher NO_3^- concentrations at depth and slower turnover rates lead to a higher f-ratio below the 10% light level.
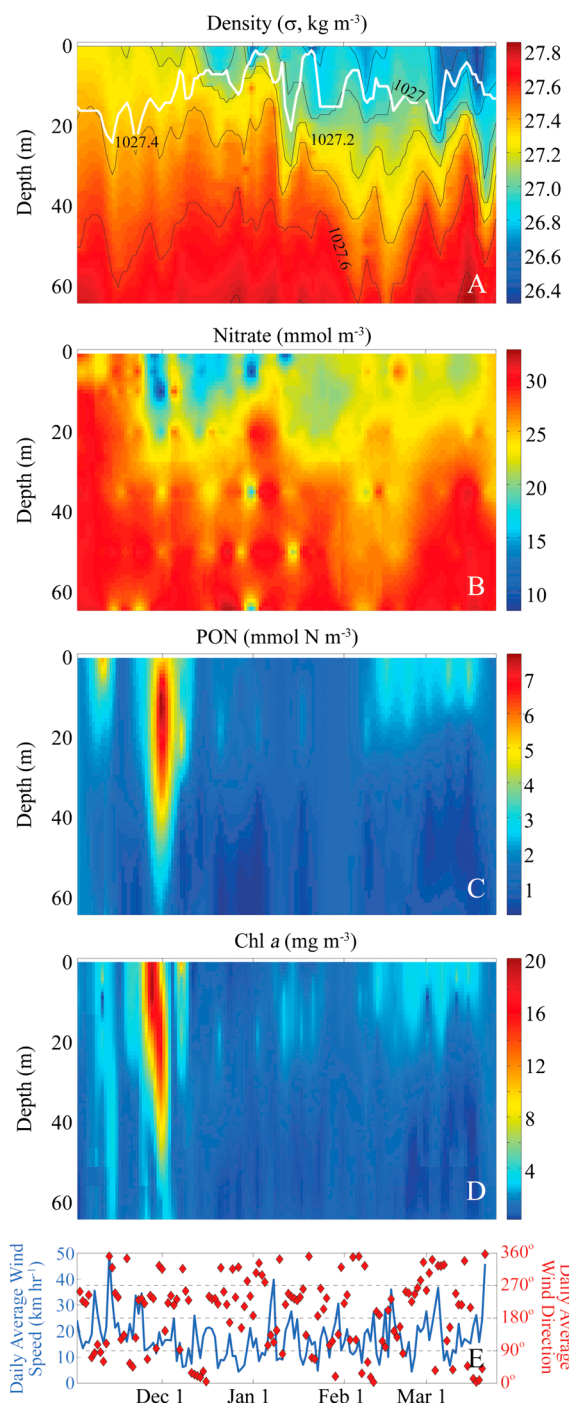
Figure 2. (a) Density ($kg\,m^{-3}$ greater than 1000). Black lines are isopycnals. White line is the mixed layer depth using the $\Delta\sigma_t > 0.125\,kg\,m^{-3}$ criterion. (b–d) Nitrate, particulate nitrogen, and chlorophyll *a* concentrations, respectively. All interpolations were done by ordinary kriging as described in the methods. White dots show sampling dates and depths. (e) Daily averaged wind speed (blue) and direction (red) measured at Outcast Island (near Station E).

3. Results

3.1. 2012–2013 Field Season Characteristics

The field season for this study extended from 31 October to 25 March (a total of 145 days). Prior to our first measurements, sea ice filled the region, preventing sampling and likely severely restricting phytoplankton growth. When the ice retreated (driven by offshore winds), surface NO_3^- concentrations were high (25–30 $\mu mol\,L^{-1}$), phytoplankton biomass was low (Chl *a* concentrations were between 1.5 and 2 $\mu g\,L^{-1}$) and the mixed layer depth (MLD, defined as $\Delta\sigma_t$ of 0.12 $kg\,m^{-3}$) was 17 m (Figure 2). Surface seawater density decreased throughout the season due to a combination of surface warming and introduction of freshwater through ice melt and precipitation, leading to increased stratification. A strong diatom bloom (peak Chl *a* concentrations >20 $\mu g\,L^{-1}$) at Stations E and B formed in late November following a low wind, high irradiance period. The bloom drew surface NO_3^- concentrations down to ~10 $\mu mol\,L^{-1}$ and led to the accumulation of significant PN standing stocks (>8 $\mu mol\,N\,L^{-1}$). The bloom was short-lived at Station E, however, ending abruptly in early December. The bloom lasted roughly 9 days longer at Station B but also suffered a rapid decline. Following, the bloom crash, nutrients returned to values >20 $\mu mol\,L^{-1}$, probably as a result of upwelling or mixing events in late December. However, despite abundant sunlight and nutrients (Figure 3), phytoplankton concentrations remained low through the end of January, with a community dominated by cryptophytes [Young et al., 2014]. In mid-February a secondary phytoplankton bloom (mixed diatoms and *Phaeocystis*) formed more gradually over the upper 10 m of the water column and lasted until mid-March, reaching peak concentrations of 4–5 $\mu g\,L^{-1}$ (Figure 2d).

3.2. Phytoplankton Production and NO_3^- Uptake

^{14}C primary production (^{14}C-PP) and nitrate uptake measurements largely followed the course of the phytoplankton bloom, with both variables peaking in late November and attaining maximum values of 439 $mg\,C\,m^{-3}\,d^{-1}$ and 85 $mg\,N\,m^{-3}\,d^{-1}$ (Figure 4). The *f* ratios were near 1 during the bloom, indicating that the phytoplankton community was growing almost entirely on NO_3^-. Following the bloom crash, ^{14}C-PP and NO_3 uptake remained low through
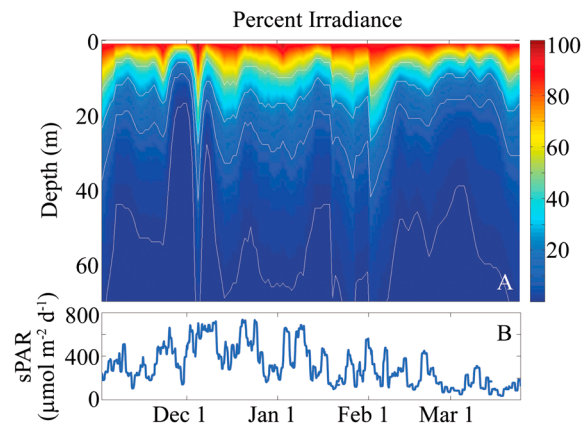
Figure 3. (a) The percent surface irradiance reaching depths throughout the season. White lines show the 50%, 25%, 10%, and 1% light levels. (b) Surface irradiance.

most of December and January. In early February and into March, phytoplankton biomass, ^{14}C-PP, and NO_3 uptake increased slowly, in conjunction with the secondary late summer bloom. During the late summer bloom, modeled weekly f ratios ranged from 0.22 to 0.37 and were significantly lower than f ratios during the main spring bloom (modeled weekly f ratios of 0.64–0.76), suggesting that phytoplankton were only deriving approximately one quarter to one third of their N from NO_3^- later in the season.

To account for the fact that light absorption changed significantly during the season (with the 1% light level shoaling to less than 20 m at the peak of the bloom; Figure 3), we estimated primary production (PP$_{model}$) and nitrate uptake (NP$_{model}$) using the models:

$$PP_{model} = P_{max} \times \tanh(PAR/I_k) \quad \text{and} \quad NP_{model} = f \times PP_{model}.$$

Our irradiance-corrected model primary and new production largely agreed with our incubation measurements, from which the model parameters were derived, indicating relatively minor bias introduced by the choice of light levels (Figure 5). However, during the main spring bloom, and to a lesser extent the smaller late summer bloom, the light-corrected model predicted less production than the measurements, because the samples were actually incubated at higher irradiance than the in situ communities experienced. PP$_{model}$ reached a peak of $4405 \, mg \, C \, m^{-2} \, d^{-1}$ in late November, a low peak of $180 \, mg \, C \, m^{-2} \, d^{-1}$ in late December, and averaged $2015 \, mg \, C \, m^{-2} \, d^{-1}$ through the late summer bloom from early February to mid-March. Throughout our measurement season, PP$_{model}$ averaged $1491 \pm 176 \, mg \, C \, m^{-2} \, d^{-1}$ and NP$_{model}$ averaged $105 \pm 17 \, mg \, N \, m^{-2} \, d^{-1}$, which would equate to an f ratio of 0.40 ± 0.08 if we assumed Redfield 106:16 C:N molar ratio for phytoplankton. For the first portion of the growth season, we compared NP$_{model}$ to new production rates that would be calculated from NO_3^- drawdown. When calculated from the beginning of our measurements until November 29 (the date of maximum NO_3^- drawdown), NO_3^- measured drawdown was $5278 \pm 340 \, mg \, N \, m^{-2}$ (mean $182 \, mg \, N \, m^{-2} \, d^{-1}$; Figures 5g and 5h) compared to NP$_{model}$ of $6398 \pm 1554 \, mg \, N \, m^{-2}$ (mean $221 \, mg \, N \, m^{-2} \, d^{-1}$). Thus, our modeled estimates of NP were within 21% of the values derived from NO_3^- deficit calculations.

3.3. Sediment Trap Export

Compared to nitrate uptake, sediment trap fluxes showed relatively low temporal variability (coefficient of variation was 0.33 for sediment traps compared to 0.86 for NP$_{model}$) in both the small- and large-size particle fractions (Figure 6). Total N flux varied from 7.2 to $24.6 \, mg \, N \, m^{-2} \, d^{-1}$, although it is important to note that the sediment trap was not deployed at Station E when the bloom crashed. The
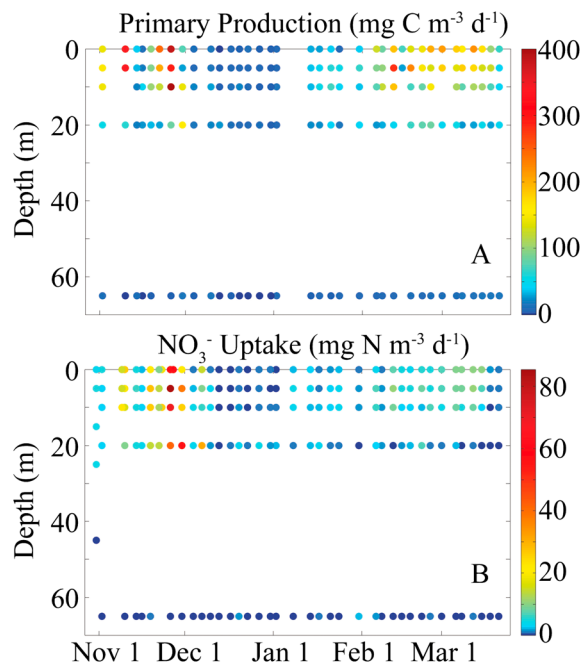

Figure 4. Phytoplankton production measurements. (a) ^{14}C primary productivity measurements at Station E. (b) ^{15}N nitrate uptake measurements. Samples were incubated for 24 h at 100%, 50%, 25%, 10%, and 0% light levels for depths 0, 5, 10, 20, and 65 m, respectively. Note the different color scales in Figures 4a and 4b.
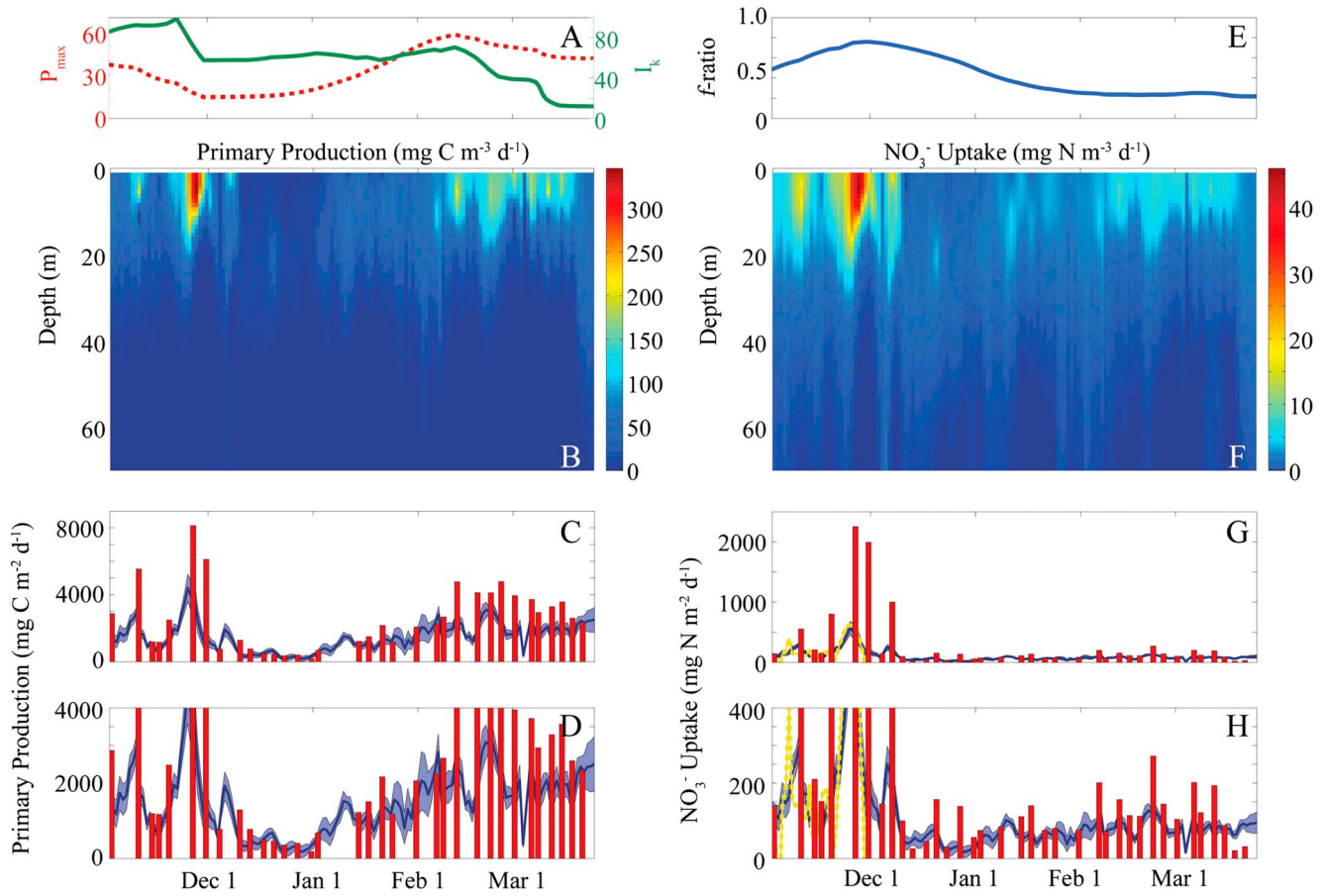
Figure 5. Phytoplankton productivity models. (a) Two-week exponentially weighted moving averages of P_{max} and I_k derived from irradiance, chl, and ^{14}C-PP measurements (fitting the equation: PP = P_{max} × Chl × tanh(PAR/I_k)). (b) Our estimates of in situ primary production derived from the model with these parameters. (c and d) A comparison of vertically integrated (to 65 m) model PP (dark blue line is mean; light blue areas show ±SD) with vertically integrated measured PP (red bars) from incubations without light level corrections. The y axes in Figures 5c and 5d are scaled differently to highlight the high productivity (Figure 5c) and low productivity (Figure 5d) periods. (e–h) Equivalent to Figures 5a–5d but for nitrate uptake using the model: NP = f × PP. Figure 5e shows the f ratio, Figure 5 shows the modeled nitrate uptake, and Figures 5g and 5h show vertically integrated measured nitrate uptake. In Figures 5g and 5h, the dashed yellow line shows nitrate drawdown calculated as the negative rate of change of vertically integrated [NO_3^-] from the beginning of the season until the point of lowest nitrate concentration (29 November).
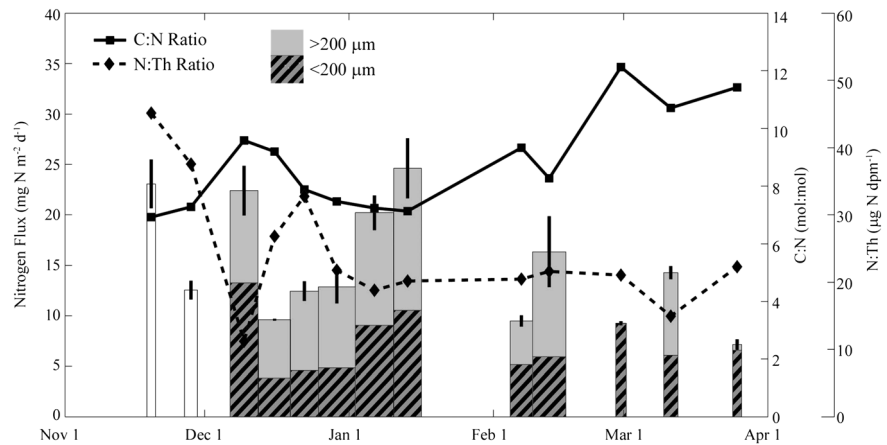

Figure 6. Nitrogen fluxes into the sediment traps moored at Station B (November and March deployments) and Station E (December–February deployments). Bar plots show vertical flux of N into the traps. Duration of trap deployment is indicated by the width of the bar. Solid gray area is the flux of >200 μm particles (primarily krill fecal pellets), and hashed bars are the flux of <200 μm particles. For the first two deployments particles were not size fractionated. Dashed line is the N:[234]Th ratio of particles collected in the trap. Solid line is the C:N ratio (mol:mol).
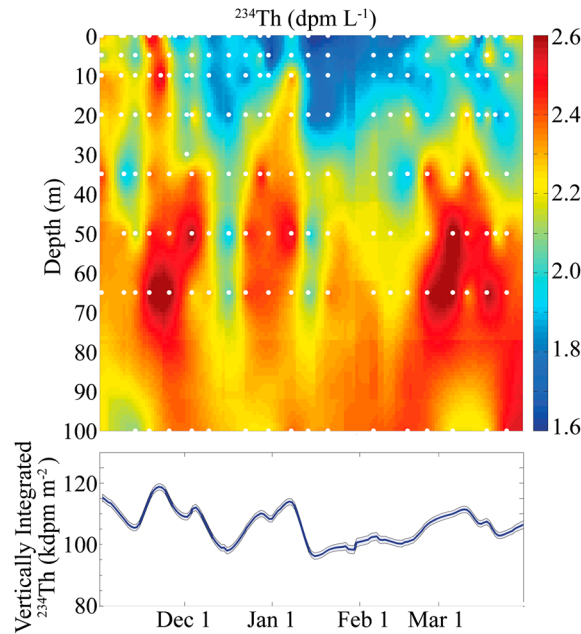
Figure 7. ^{234}Th activity (decays min^{-1} L^{-1}) during the seasonal cycle at Station E as a function of depth from November through March. Interpolation was done by ordinary kriging. White dots show sampling dates and depths. Lower plot is vertically integrated (to 50 m) ^{234}Th deficiency (dpm m^{-2} d^{-1} × 1000).

fraction of $>200\,\mu$m particles in the sediment trap (comprised almost entirely of recognizable krill fecal pellets) varied from 0 to 64%, highlighting the variable importance of fecal pellets to sediment trap flux. The C:N ratio of trap material increased over the course of the season, from a low of 6.9 mol:mol to a high of 12.1 mol:mol. By contrast, the N:Th ratio showed a less consistent seasonal trend, with relatively lower ratios during periods of higher biomass. The mean N:^{234}Th ratio for the season was 24.2 (±9.3 standard deviation) μg N dpm^{-1}.

3.4. ^{234}Th Export

Throughout the field season, water column ^{234}Th activity was typically measured weekly, with a 22 day gap from 21 January to 12 February during the cruise. At the beginning of the season (2 November), ^{234}Th concentrations in the upper 20 m were near equilibrium with ^{238}U (which remained near 2.4 dpm L^{-1} throughout the season), with deficiencies of between 0 and 0.3 dpm L^{-1}. While ^{234}Th concentrations below 50 m remained near equilibrium with ^{238}U throughout the season, surface ^{234}Th concentra-

tions decreased steadily in early November and then rapidly following the crash of the bloom at the end of November (Figure 7). Surface water ^{234}Th concentrations remained low throughout January, although with some variability possibly related to upwelling of high ^{234}Th concentration water from depth. During late February and March the ^{234}Th concentrations in surface waters began to increase, although as of our latest sampling date (25 March), ^{234}Th had not returned to equilibrium with ^{238}U, and deficiencies in the upper 20 m remained in the range of 0.1 to 0.5 dpm L^{-1}. A full budget for water column ^{234}Th activity can be written as

$$\frac{\partial^{234}\text{Th}}{\partial t} = \left(^{238}\text{U} - ^{234}\text{Th}\right)\lambda_{234} - E + V_{\text{vertical}} + V_{\text{lateral}} \tag{4}$$

where ^{234}Th and ^{238}U are the vertically integrated (to 50 m for consistency with all other vertically integrated measurements in this manuscript) activities of the respective isotopes, λ_{234} is the decay constant for ^{234}Th, E is the export of ^{234}Th on sinking particles, and V_{vertical} and V_{lateral} are the net advective plus diffusive inputs of ^{234}Th to the study region (Figure 8). This equation can be solved for export:

$$E = ^{234}\text{ThProduction} + \text{NSS}_{\text{term}} + \text{NetAdvectiveDiffusive} \tag{5}$$

to show that total ^{234}Th export is the sum of a component representing the net production of ^{234}Th from ^{238}U, a nonsteady state (NSS) term, and the net vertical and horizontal thorium inputs, where

$$^{234}\text{ThProduction} = \left(^{238}\text{U} - ^{234}\text{Th}\right)\lambda_{234} \tag{6}$$

$$\text{NSS}_{\text{term}} = \frac{-\partial^{234}\text{Th}}{\partial t} \tag{7}$$

$$\text{NetAdvectiveDiffusive} = V_{\text{vertical}} + V_{\text{lateral}} \tag{8}$$

Typically, it is assumed that ^{234}Th is at steady state, with minimal advective and diffusive inputs, and hence, export can be solved from the deficiency of ^{234}Th from ^{238}U. However, our time series clearly indicates that ^{234}Th concentrations were not at steady state. We must thus calculate $\partial^{234}\text{Th}/\partial t$ from our ^{234}Th profiles (Figure 7). If we then assume that vertical and horizontal advective inputs are minimal, we can solve for export using a NSS equation with no advection or diffusion (Figure 9b):

$$E = \left(^{238}\text{U} - ^{234}\text{Th}\right)\lambda_{234} - \frac{\partial^{234}\text{Th}}{\partial t} \tag{9}$$

Nitrate Mass Balance

$$\frac{\partial NO_3^-}{\partial t} = \int_{z=0}^{50} \text{Upwelling} \times \frac{\partial NO_3^-}{\partial z} dz - \text{NitrateUptake} + \text{EuphoticNitrification}$$

^{234}Th Mass Balance

$$\frac{\partial ^{234}Th}{\partial t} = \left(^{238}U - ^{234}Th\right)\lambda_{234} + \int_{z=0}^{50} \text{Upwelling} \times \frac{\partial ^{234}Th}{\partial z} dz - \text{Export}$$

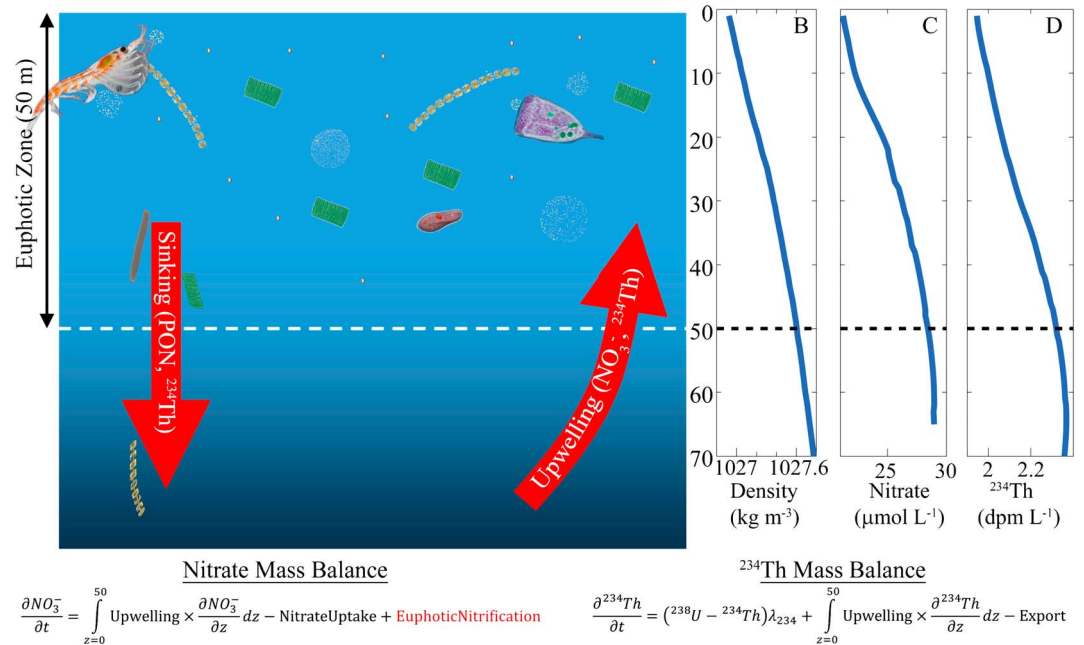**Figure 8.** (a) Schematic diagram showing the related budgets of NO_3^- and ^{234}Th, assuming that NO_3^- is only introduced to the surface ocean by upwelling. (b–d) Season-average vertical profiles of density, NO_3^-, and ^{234}Th (though note that when calculating fluxes season-average profiles were never used, we always used temporally varying profiles as found in Figures 2 and 7). NO_3^- and ^{234}Th mass balance equations are written out below. Note that shallow water nitrification is written in red as we assume that it is negligible in our initial budgets (but see our discussion).

Multiplying the estimated ^{234}Th export from equation (9) by the mean N:^{234}Th ratio from the sediment traps (24.2 μg N dpm^{-1}) yields the ^{234}Th-based sinking N export for comparison with sediment traps. While there is a significant amount of error in this calculation due to our high temporal resolution ^{234}Th sampling, it is important to note that this error term refers to the export at any one given day. When integrated over the seasonal cycle, the NSS error term disappears almost entirely, as does most of the effect of the NSS term, since ^{234}Th concentrations at the end of the season were only slightly less than ^{234}Th concentrations at the beginning of the season. Averaging over the full field season yields an estimate of 10.5 ± 1.2 mg N m^{-2} d^{-1}, which compares favorably with the magnitude of flux into our sediment traps (mean 14.9 mg N m^{-2} d^{-1}, standard deviation 5.9 mg N m^{-2} d^{-1}). However, it is important to note that this estimate neglects any advective inputs (or losses) of ^{234}Th. Upwelling in particular may be important, given the apparent upwelling event that may have introduced NO_3^--rich Upper Circumpolar Deep Water onto the shelf near Palmer Station at the end of the spring phytoplankton bloom [*Tortell et al.*, 2014].

To estimate the input of ^{234}Th by upwelling, we used a NO_3^- mass balance approach for the upper 50 m to estimate temporally varying upwelling rates (Figure 8):

$$\frac{\partial NO_3(t)}{\partial t} = -\int_{z=0}^{50} NP_{model}(t)dz + \int_{z=0}^{50} \text{Upwelling}(t) \times \frac{\partial NO_3}{\partial z} dz \qquad (10)$$

where NP_{model} is our modeled NO_3^- uptake (see phytoplankton production section above) and $\partial NO_3/\partial z$ was calculated as the vertical gradient over the upper 50 m. We then used this upwelling rate and the vertical gradient of ^{234}Th (both vertical gradients determined by linear regression of measurements made in the upper 50 m) to estimate the vertical advective input and solve a full NSS with advection equation to determine ^{234}Th export:

$$E(t) = \left(^{238}U(t) - ^{234}Th(t)\right)\lambda_{234} - \frac{\partial ^{234}Th(t)}{\partial t} + \int_{z=0}^{50} \text{Upwelling}(t) \times \frac{\partial ^{234}Th(t)}{\partial z} dz \qquad (11)$$

By solving for this equation, we find that $V_{vertical}$ (the upwelling term) is a significant term in the ^{234}Th budget at Station E. ^{234}Th export calculated with the NSS equation and correction for upwelling (Figure 9c and equation (7)) is 1.9 times greater than with the NSS equation alone (Figure 9d and equation (9)), leading to a
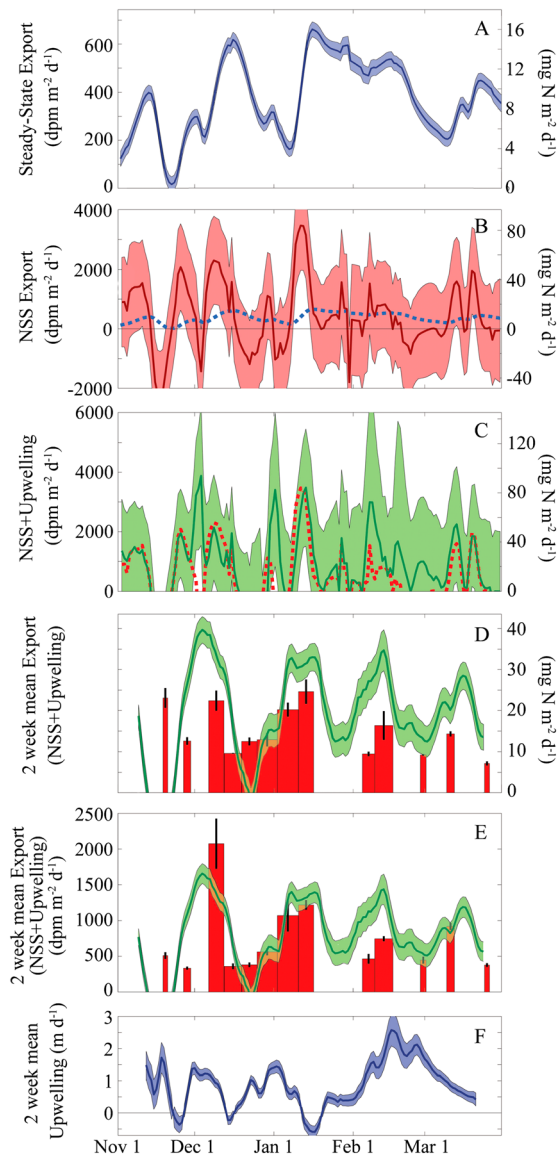
Figure 9. ^{234}Th export during the seasonal cycle at Station E. The export calculated with (a) a simple steady state equation, (b) a nonsteady state (NSS) equation, and (c) a NSS equation with upwelling. In each plot, left y axis is the calculated export of ^{234}Th and right y axis is the nitrogen export (assuming a constant N:^{234}Th ratio throughout the season). The shaded area in each plot shows the uncertainty of the estimate. In Figure 9b, blue dashed line shows the steady state estimate and in Figure 9c, the red dashed line shows the NSS estimate without upwelling. (D) Plot shows export calculated for a NSS equation with upwelling as in Figure 9c but shows 2 week averaged export around any given date (green line), which significantly decreases the error associated with changes in properties in time. Red bars show the sediment trap export. We show only the N flux on this graph to avoid confusion since the N:^{234}Th collected in the traps varied. (e) Plot, same as Figure 9d but now showing flux in ^{234}Th units so that collection efficiency of the traps can be directly compared. (f) The 2 week average upwelling computed to determine the export estimates in panels D & E. Note that this upwelling term is calculated under the assumption that upwelling is the only process transporting nitrate and ^{234}Th into the surface ocean from depth.

mean export estimate of 20.4 ± 2.4 mg N m^{-2} d^{-1} during the period from 2 November to 26 March. It is important to note that the large error bars in Figure 9c are associated with our uncertainty in estimating export on any given day, due to the large uncertainties inherent to estimating short temporal scale changes in ^{234}Th. If we instead use the same equation to estimate the 2 week mean ^{234}Th export around any given time, we find that our uncertainty shrinks considerably and we can derive a more accurate depiction of the temporal pattern of export at Station E (Figure 9d). We find that export peaked at a rate of 39.7 ± 3.4 mg N m^{-2} d^{-1} during a 2 week period centered around 4 December at the end of the bloom. However, there were also sizable export events in early January and mid-February.

The overall magnitude of fluxes estimated by ^{234}Th with the NSS and upwelling terms (equation (11)) and the sediment trap was relatively similar (using point-to-point matchups, the ^{234}Th-based approach yielded a median 1.4X greater flux). However, the ^{234}Th-based approach suggested significantly greater temporal variability than the sediment trap-based estimate (Figure 9e). Using a type II linear regression, the correlation coefficient between the sediment traps and ^{234}Th was 0.29, although it increased to 0.70 if we exclude data from the first sediment trap deployment, which occurred during a 2 day period when heavy sea ice drifted through the study region and actually dragged the trap mooring several hundred feet. The ^{234}Th-based approach also has a significant advantage in that it gives us continuous coverage of the study region, while sea conditions at times prevented us from deploying the sediment trap.

3.5. Comparison of New, Net Community, and Export Production

In addition to the two methods of determining new production (NO$_3^-$ uptake and net NO$_3^-$ drawdown) and two methods of determining sinking particle flux (^{234}Th and sediment traps) at Station E, we also measured O$_2$:Ar ratios at the seawater intake near Palmer Station ([*Tortell et al.*, 2014, Figure 4] converted to N units assuming a Redfied ratio of 106:16 C:N and multiplied by the mixed layer depth) as a measure of net community production (NCP). NCP, the balance between photosynthesis and respiration, should be functionally similar to
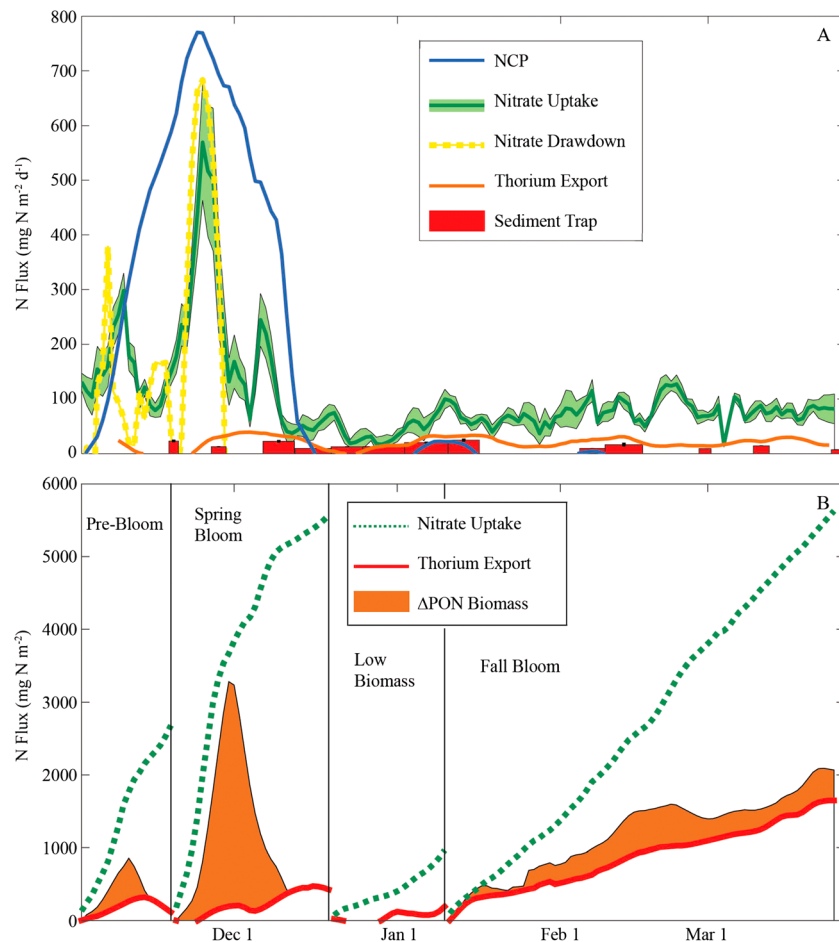
Figure 10. Comparison of new production, net community production, and export near Palmer Station. (a) O_2/Ar net community production (blue) at the seawater intake, nitrate uptake (dark green with light green error bars) at Station E, nitrate drawdown (yellow dashed line) at Station E, nitrogen export determined by [234]Th (orange) at Station E, and nitrogen export determined by sediment trap (red bars) at Stations B and E. NCP was calculated from O_2:Ar ratios measured at the Palmer Station seawater intake and converted from O_2 to N units by assuming Redfield stoichiometry. (b) Cumulative export integrated over four distinct periods during our field season (prebloom, bloom, low biomass period, and fall bloom). Red line shows export calculated by [234]Th. Brown area plot shows the net increase in PN between any given time point and the beginning of the respective period. Green dashed line shows cumulative nitrate uptake. All rates are integrated to a constant 50 m depth horizon, except NCP which is integrated over the mixed layer.

new production, and we find good agreement between NCP and new production magnitudes during the peak of the bloom (Figure 10a). The longer bloom duration suggested by O_2/Ar-based NCP relative to new production likely reflects the different temporal dynamics of the sampling locations for these two variables. Whereas O_2/Ar ratios were measured in the seawater supply at Palmer Station, NO_3^- uptake was measured at Station E, 4 km offshore. Comparison of the seasonal time series for these locations shows that the phytoplankton bloom lasted significantly longer near the seawater intake than at Station E. This result could explain the fact that O_2/Ar-derived NCP remained high for a longer period than new production derived from NO_3^- uptake measurements. During the second bloom (smaller bloom) later in the season, we saw no similar increase in NCP and the O_2:Ar ratio method suggested a balance of respiration and photosynthesis or perhaps even slight net heterotrophy. This could be due to heterotrophic consumption of dissolved organic matter produced earlier in the season, but is more likely to be a methodological underestimate driven by the physical introduction (whether upwelling, vertical mixing, or tidal mixing) of lower O_2 water that we could not account for with our measurements. In contrast to the relatively close agreements between nitrate drawdown, nitrate uptake, and O_2/Ar-derived NCP, both estimates of export (sediment trap and [234]Th) were substantially lower than new production during the spring and fall blooms (Figure 10a).
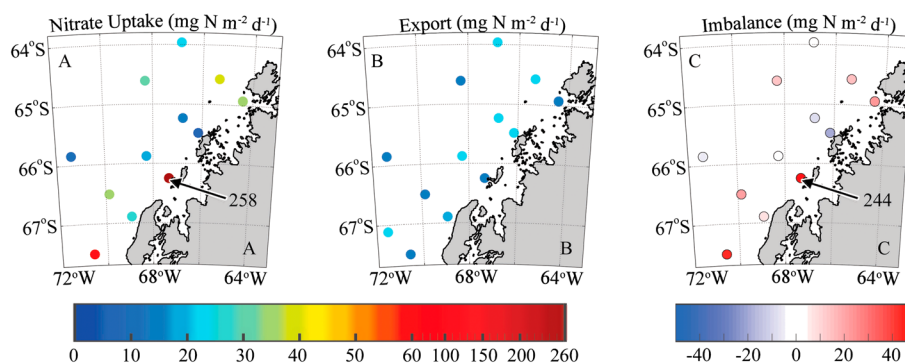
Figure 11. Ship-based estimates of new and export production in the northern WAP in early Jan 2013. (a) Nitrate uptake (note the extremely high value of 258 mg N m^{-2} d^{-1} at a coastal site). (b) Export rates (derived from ^{234}Th disequilibrium with a steady state assumption). (c) The imbalance of new and export production (note the point of 244 mg N m^{-2} d^{-1} at a coastal site, which was greater than our color axis).

A strict in situ balance of new and export production (defined in this context as sinking particulate nitrogen flux only, but see discussion) would suggest that over the course of a bloom cumulative new production will be balanced by the sum of the net increase in PN (since the beginning of the bloom) and export (Figure 10b). We have divided the season into four distinct periods: (1) prebloom (1–18 November) was characterized by a brief spike in new production that rapidly crashed; (2) spring bloom period (19 November to 18 December, which includes postcrash export) saw the highest PN increase, which accounted for almost all new production from the beginning of the bloom until its peak; (3) low biomass period (19 December to 9 January) that had decreased levels of new production, biomass, and export; and (4) fall bloom (10 January to 24 March) that sustained moderate levels of new production for >2 months with a slow buildup of PN. Despite the significant seasonal variability, each phase of the growth season showed a strong surplus of new production relative to export (Figure 10b). Over the course of the season, NO$_3^-$ uptake was a factor of 5.3 greater than thorium-based N export.

3.6. Basin-Wide ^{234}Th and NO$_3^-$ Uptake

During early January, f ratios throughout the northern WAP region offshore of Palmer Station were low (mean = 0.14, median = 0.10, range = 0.02–0.43). Nitrate uptake was significantly lower than the mean at Station E, except in one coastal station where vertically integrated rates reached 258 mg N m^{-2} d^{-1}. Despite these low f ratios, NO$_3^-$ uptake still substantially exceeded ^{234}Th-based export (calculated with a one-dimensional steady state assumption) for the region (Figure 11). Region-wide NO$_3^-$ uptake averaged 47.9 ± 14.4 mg N m^{-2} d^{-1} compared to a region-wide mean export (for the same stations) of 19.9 ± 1.4 mg N m^{-2} d^{-1} (range 14.7–25.4). Production exceeded export at 8 of 12 stations. At one coastal site where export exceeded production, export was relatively moderate (25 mg N m^{-2} d^{-1}), but the f ratio was exceedingly low (0.02) despite high NO$_3^-$ concentrations, leading us to wonder if there was a problem with the nitrate uptake incubations at this station. Nevertheless, it is clear that new production substantially exceeded export in the wider study region, as it did near Palmer Station.

4. Discussion

Over 80% of the new production at Palmer Station could not be accounted for by our export measurements. Even if we assume that some production is laterally exported from the coastal region to the shelf as in other coastal upwelling regions [Olivieri and Chavez, 2000; Plattner et al., 2005; Stukel et al., 2011], the fact remains that regional export was only 42% of new production across the WAP grid of stations during the January cruise. The cruise corresponded with a seasonal low in local primary production at Palmer Station, indicating that the imbalance may have been even greater earlier in the season. In this discussion we will focus first on the potential for methodological biases that introduce uncertainty into our production and export estimates. We will then discuss several potential losses of N (to higher trophic levels, migration, DON accumulation, and vertical mixing) from the ecosystem.
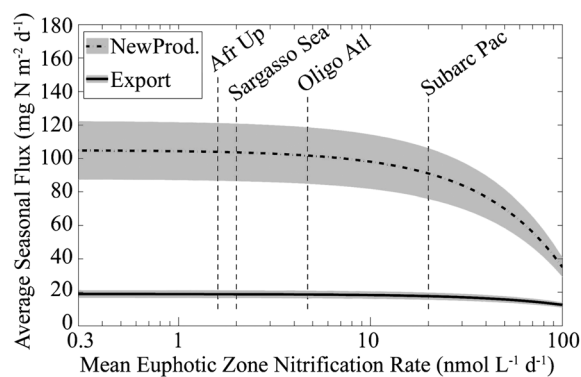
Figure 12. The impact of shallow water nitrification rates (x axis is logarithmic) on our estimates of new production and vertical nitrogen flux. Vertical dashed lines are mean nitrification at the 55% light level in the African Upwelling region [*Clark et al.*, 2008], maximum ammonium oxidation rates in the Sargasso Sea [*Newell et al.*, 2013], mean nitrification at the 55% light level in the oligotrophic Atlantic [*Clark et al.*, 2008], and mean ammonium oxidation rates in the Subarctic Pacific [*Grundle et al.*, 2013].

4.1. The Imbalance of New and Export Production: Is It a Methodological Bias?

The use of the $^{15}NO_3^-$ uptake method to estimate new production rests on the assumption that NO_3^- is not recycled in the ecosystem, but instead is supplied only by upwelling and vertical mixing, with nitrification occurring beneath the euphotic zone [*Dugdale and Goering*, 1967]. This simplifying assumption was based on the belief that nitrification was inhibited by light [*Olson*, 1981; *Ward et al.*, 1982], but shallow water nitrification has since been found to be a common, and at times potentially dominant, source of nitrate to stratified, oligotrophic ecosystems [*Yool et al.*, 2007]. Figure 12 shows the relative impact of reasonable average euphotic zone nitrification rates on our estimates of new production and export (note that the export term is also influenced because shallow nitrifica-

tion decreases the calculated upwelling; Figure 8 and equations (11) and (12)). Given the cold temperatures and high NO_3^- concentrations in surface waters in the WAP, it seems unlikely that nitrification is supplying much of the nitrate inventory. Indeed, investigations of nitrate isotopes in the Ross Sea suggested that shallow water nitrification rates were less than 6% of nitrate uptake rates [*DiFiore et al.*, 2009]. We can also address the potential importance of mixed layer nitrification, by examining NO_3^- dynamics during the spring bloom period. During late November nitrate uptake was entirely consistent with nitrate drawdown, PN biomass increase, and net community production (Figure 10). Following the bloom, PN decreased rapidly (time scale ~1 week) and surface nitrate concentrations rebounded from $<10\,mmol\,m^{-3}$ to $>20\,mmol\,m^{-3}$ over the course of a month, despite continued nitrate uptake. Even if the continued nitrate uptake were neglected, this would equate to a nitrification rate on the order of 0.5 $\mu mol\,L^{-1}\,d^{-1}$, which is more than an order of magnitude higher than typical euphotic zone nitrification rates. Nevertheless, for the late summer bloom period, when O_2:Ar measured NCP remained low and nitrate concentrations remained high, shallow water nitrification remains a potential (though unlikely) alternative to the more likely explanation of persistent vertical inputs of nitrate-rich and oxygen-poor water.

Another potential error source comes from our use of a model to account for our constant light level incubations despite a significant change in in situ light levels. It is important to note first that our model led to a substantially reduced estimate of new production (i.e., helping to close the imbalance) relative to our raw measurements. Furthermore, the model parameter values that we derived for P_{max} and I_k agreed well with the region-wide means independently estimated by *Moline et al.* [1998]. Again, the agreement between our modeled nitrate uptake and both PN accumulation and nitrate drawdown during the strong spring bloom lends further credence to our estimate of new production, at least during this period. New production during this 2 week bloom was greater than total export during the entire 5 month season.

As with new production, there is uncertainty added into our estimate of export by the use of our nonsteady state with upwelling model of ^{234}Th cycling. But as with new production, the application of the model serves to narrow the gap between new and export production (by increasing export estimates) relative to a simpler (steady state, no vertical inputs of ^{234}Th) interpretation of the in situ data. We note that alternative models could have led to even higher export. For example, an estimate of increased upwelling rates would have led to correspondingly increased ^{234}Th fluxes, but that would have been inconsistent with the water column NO_3^- budget. An alternative coastal upwelling model could be used in which upwelling is restricted to regions inshore of Station E thus leading to horizontal advection of water from the coast toward Station E. However, monthly measurements at Station B consistently showed slightly lower ^{234}Th concentrations than at Station E, suggesting that offshore advection would actually lead to slightly lower export estimates, exacerbating the imbalance. Furthermore, there was a relatively good agreement between the sediment traps and ^{234}Th export, and the corroboration of two independent measurements of export gives us some confidence in our results.

Another potential methodological uncertainty would arise if our estimate of the N:^{234}Th ratio was not representative of the particles being exported. N:^{234}Th (or C:^{234}Th) ratios can vary significantly with season, location, depth, and ecosystem state [*Buesseler et al.*, 2006; *Passow et al.*, 2006]. We have chosen to utilize a single N:^{234}Th ratio for the entire season, because we observed no significant trend over the course of the season. However, it is important to note that N:^{234}Th ratios were actually lower than average during the high export period of the spring bloom (Figure 6). Application of a temporally varying N:^{234}Th ratio would have led to a slight decrease in calculated N flux (using temporally varying N:Th ratios, seasonally averaged gravitational flux would be 16.3 ± 1.2, compared to 20.4 ± 2.4 mg N d^{-1} with a constant N:Th ratio), acting to further increase the discrepancy between new production and vertical fluxes. Our average C:^{234}Th ratio (177 µg C dpm^{-1}) also fell on the slightly high end of the values measured by *Owens* [2013] on two cruises in the WAP. However, it is important to note that mesozooplankton in other regions have been measured to have very high C:^{234}Th ratios (Stukel et al., in review), which means that export mediated by any trophic levels feeding upon them will be essentially invisible to ^{234}Th-based methods. Since our sediment traps (with baffle openings of ~1.25 cm) were likely to have a sampling bias against the carcasses of mesozooplankton or fecal pellets of organisms feeding on them, it is important to consider export mediated by higher trophic levels as unmeasured by our methodology. Potential export mediated by higher trophic levels will be addressed in the following section.

4.2. The Imbalance of New and Export Production: Ecosystem Considerations

The assumption that vertical flux of sinking particles is responsible for all N export from the ecosystem is, of course, an oversimplification. Several other ecosystem processes could contribute to a net flux of N from the surface waters of the coastal WAP including: diel vertical migration and lateral migrations of mesozooplankton, trophic transfer to higher trophic levels (HTL), export to land by seabirds and seals, and passive transport of dissolved organic matter. While these mechanisms were not directly addressed during our study, we can estimate the potential magnitudes of these fluxes.

Transport to HTL (fish, seals, and seabirds) can result in the production of large fecal pellets that sink in the sea (but are "invisible" to ^{234}Th and our sediment traps as explained above), biomass accumulation, or a net export of material to the land. The WAP is a productive ecosystem, with abundant large sea life. However, in coastal regions most fluxes to HTL are mediated by trophic links through krill. Thus, by estimating krill production we can put an upper limit on HTL production. While it is difficult to measure secondary production in situ, we can derive an indirect estimate of krill grazing rates. *Euphausia superba* (the dominant krill in the region) produces rapidly sinking fecal pellets which were readily observable as essentially the sole component of the >200 µm size fraction in our sediment traps. High sinking rates and low remineralization of WAP fecal pellets suggest that fecal pellet production is quantitatively linked to vertical flux; thus, our measurement that >200 µm particles comprised 50% of sinking material collected in our sediment traps (which were relatively efficient collectors of sinking material as determined by our ^{234}Th measurements) gives an estimate of mesozooplankton egestion near Palmer station of ~10 mg N m^{-2} d^{-1}.

$$\text{Grazing}_{\text{Krill}} = \frac{\text{Egestion}}{\text{EE}} = \frac{\text{FecalPelletFlux}}{\text{EE}}. \tag{12}$$

Mesozooplankton egestion efficiencies (EE, equals one minus assimilation efficiency) are typically in the range of 30% [*Conover*, 1966; *Cowie and Hedges*, 1996], although average *Euphausia superba* EE may be closer to 20% [*Kato et al.*, 1982].

$$\text{BiomassProduction}_{\text{Krill}} = \text{Grazing}_{\text{Krill}} \times \text{GGE} = \text{FecalPelletFlux} \times \frac{\text{GGE}}{\text{EE}} \tag{13}$$

Since gross growth efficiencies (GGE) typically have similar values as EE (typical metazoan zooplankton have a GGE slightly less than 30% [*Straile*, 1997]), total production by krill (and hence total material available to HTL) is unlikely to significantly exceed vertical flux of fecal pellets (~10 mg N m^{-2} d^{-1}). Thus, the sum total of all HTL-mediated export (certainly less than the amount HTL consume) is not large enough to close the apparent imbalance between new and export production (85 ± 17.6 mg N m^{-2} d^{-1}). While this analysis neglects flow of energy through nonkrill pathways (e.g., copepods to fish), copepod-mediated pathways likely involve more trophic steps (with significant energy loss) prior to reaching HTL and are hence less likely to contribute substantially to HTL-mediated export.
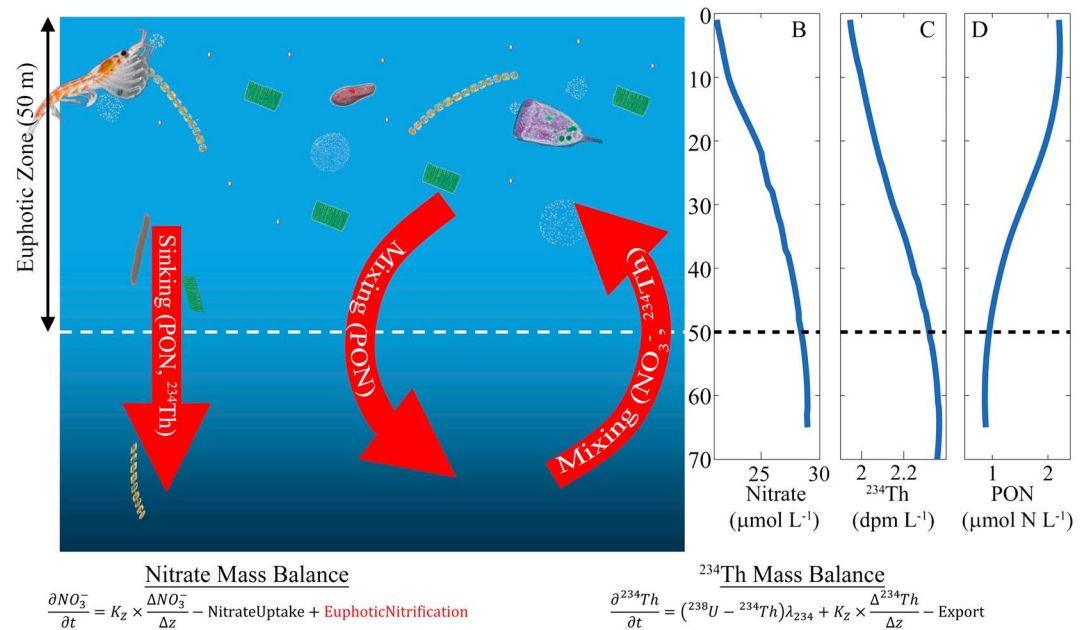
$$\frac{\partial NO_3^-}{\partial t} = K_z \times \frac{\Delta NO_3^-}{\Delta z} - \text{NitrateUptake} + \text{EuphoticNitrification}$$

$$\frac{\partial^{234}Th}{\partial t} = \left(^{238}U - {}^{234}Th\right)\lambda_{234} + K_z \times \frac{\Delta^{234}Th}{\Delta z} - \text{Export}$$

Figure 13. (a) Schematic diagram showing the related budgets of NO_3^- and ^{234}Th (as in Figure 8), but with the assumption that NO_3^- and ^{234}Th are supplied to the surface ocean only by diapycnal mixing. (b–d) Season-average profiles of NO_3^-, ^{234}Th, and PN, respectively.

Diel vertical migration (DVM) of mesozooplankton was originally considered to be an important pathway for carbon export only in oligotrophic, open ocean regions [*Steinberg et al.*, 2000; *Hannides et al.*, 2009], although it has also been found to be a substantial carbon flux in coastal regions [*Stukel et al.*, 2013]. Nevertheless, the contribution of DVM may be marginal in summer in the WAP where day-night differences in insolation are significantly less than in low-latitude regions. Krill may also transport nitrogen laterally by feeding near the coast and migrating offshore—behavior that may be enhanced in the Palmer region by tidally influenced variability [*Bernard and Steinberg*, 2013]. However, the bulk transport by vertical and lateral migration is unlikely to be substantial for the same reasons that krill secondary production and transfer to HTL cannot close the imbalance.

Dissolved organic matter (DOM) export is an export vector not captured by sediment traps or the ^{234}Th method. However, measurements of DOM in the WAP and other Southern Ocean ecosystems have not shown a significant seasonal buildup in DOM and have suggested that most production is shunted through particulate rather than dissolved pathways [*Carlson et al.*, 1998; *Hansell and Carlson*, 2002], with the implication that DOM export is a relatively minor export term in the WAP.

4.3. The Imbalance of New and Export Production: Vertical Mixing and a "Leaky" Ecosystem

In considering the input of NO_3^- necessary to sustain phytoplankton growth and close the dissolved nutrient budget, we considered NO_3^- input as a purely advective (upwelling) process. However, over the course of the season, surface density decreased (due to warming and freshening) without showing evidence of sustained upwelling and sustained upwelling favorable winds were not observed (Figure 2e; though note the brief period in mid-December with upwelling favorable winds). Diapycnal mixing is another process that can potentially introduce NO_3^- and ^{234}Th to surface waters, while simultaneously removing PN and DON out of the surface layer. Mixing has been previously shown to transport POM to depth as a result of day-night differences in MLD [*Gardner et al.*, 1993, 1995] and storm-induced mixing events [*Pesant et al.*, 2002; *Waniek*, 2003] in the North Atlantic. To consider the possible magnitude of PN export due to diapycnal mixing from the surface ocean (Figure 13), we assumed that upwelling was negligible and defined turbulent diffusive flux of NO_3^- as $J_{NO3} = K_z \times \Delta NO_3^-/\Delta z$, where K_z is the vertical eddy diffusivity and $\Delta NO_3^-/\Delta z$ is the vertical gradient in NO_3^- over the upper 65 m (calculated using a least squares linear regression with the data shown in Figure 2b). Once we combined this equation with the NO_3^- fluxes required to replace the NO_3^- taken up by phytoplankton and after accounting for temporal changes in NO_3^-, we were able to solve for K_z (Figure 14a). We then
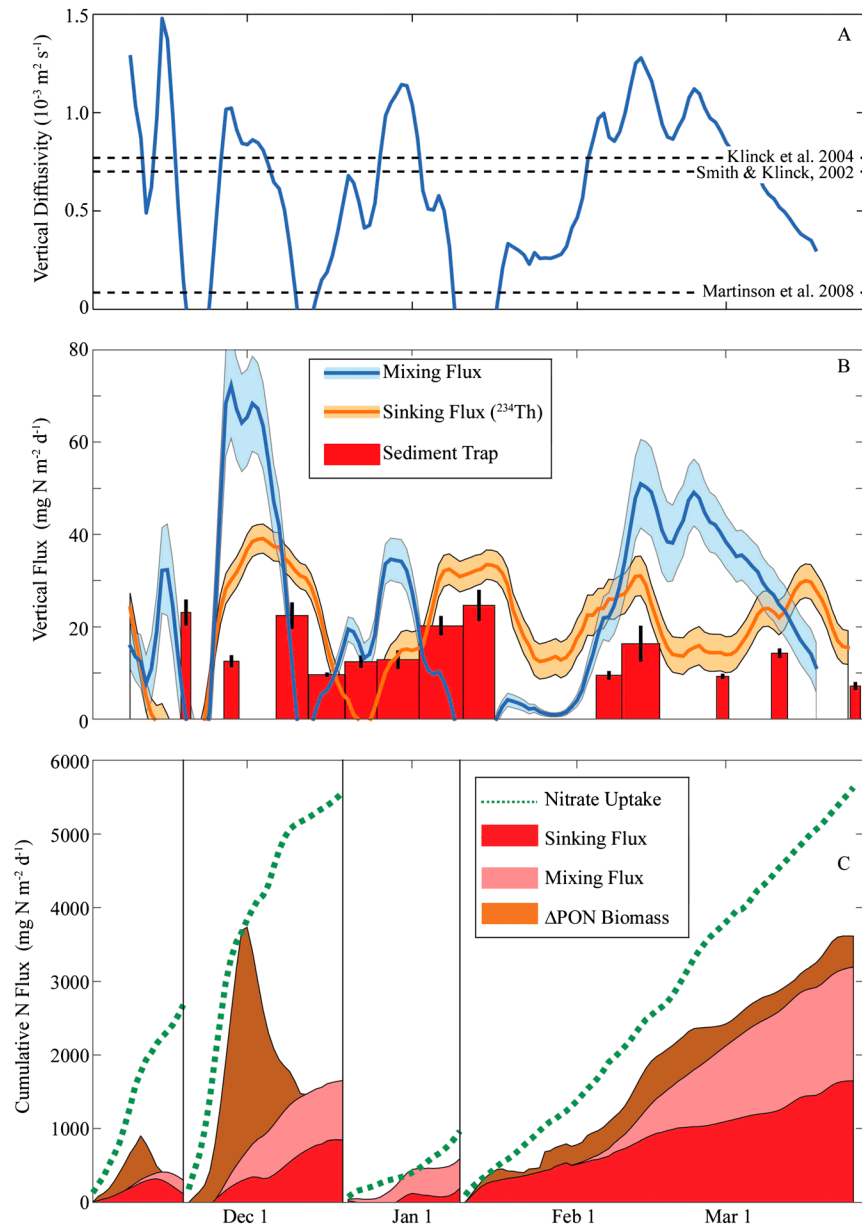
Figure 14. Comparison of new production and export at Station E under the assumption that mixing (rather than upwelling) introduces NO_3^- to the surface waters. (a) Our calculated vertical diffusivities (K_z, blue line). Dashed black lines are mean K_z estimated in other modeling studies in the region. (b) Losses of PN from the from the upper 50 m due to vertical mixing (blue line) and sinking flux (measured by ^{234}Th, orange line; measured by sediment trap, red bars). (c) A comparison of cumulative nitrate uptake to cumulative sinking and mixing fluxes and the change in PN biomass for the four time periods explained in Figure 10b.

determined an equivalent vertical gradient in PN over the upper 65 m (from data shown in Figure 2c) and calculated equivalent diffusive fluxes of ^{234}Th into the upper 50 m (to recalculate export based on our ^{234}Th measurements) and PN out of the upper 50 m (Figure 14b). While the physical mechanisms driving this vertical mixing cannot be determined from the present data, several possibilities include wind-driven mixing, breaking internal waves [*Garrett and Munk*, 1972], and icebergs [*Helly et al.*, 2011; *Smith et al.*, 2013]. Our mean K_z calculated for the season (5.6×10^{-4} m^2 s^{-1}) also compares favorably with that generated from other models in the region [e.g., *Smith and Klinck*, 2002; *Klinck et al.*, 2004; *Martinson et al.*, 2008].

When these diffusive fluxes were taken into account (and upwelling was assumed to be negligible), sinking flux of PN accounted for an average of 19.8 mg N m^{-2} d^{-1} (19% of new production) and vertical mixing of PN

to depth accounted for an additional 20.4 mg N m^{-2} d^{-1} (20% of new production), when both are averaged for the entire season. However, during the periods spanning January–March, most new production could be accounted for by the sum of these two processes (during the low biomass period sinking flux and PON mixing flux were 8.8 and 18.2 mg N m^{-2} d^{-1}, respectively, compared to nitrate uptake of 43.9 mg N m^{-2} d^{-1}; during the fall bloom the equivalent values were 22.3, 20.9, and 76.0 mg N m^{-2} d^{-1}; Figure 14c). The remaining gap would be partially bridged by the diffusive transport of DON to depth. Although we do not have DON measurements for our field season, during the 2010–2011 and 2011–2012 field seasons the median vertical DOC gradient was −0.033 mmol m^{-3} m^{-1}. If we assume Redfield C:N molar ratios and use our average vertical eddy diffusivity, the added transport of DON would be 3.3 mg N m^{-2} d^{-1}. While this is a crude estimate, it is clear that mixing of DON cannot close the entirety of the remaining gap between export and new production. In particular, there is clearly still a large discrepancy between new and export production during the spring bloom period. The end of this bloom marked the only portion of the season with sustained (though weak) offshore winds (Figure 2e), which may have led to offshore advection of surface water at the end of the bloom (as suggested by *Tortell et al.* [2014]). This offshore advection would have briefly decoupled new and export production near the coast.

If this high ratio of mixing-driven diffusive losses of PN to sinking flux of PN holds throughout the region, then combined export would be within 20% of balancing new production. This possibility has significant consequences for the ecosystem. Traditionally, the WAP has been considered a quintessential example of the classical Antarctic diatom-krill-predator food chain [*Knox*, 2006], which would be expected to be an efficiently exporting ecosystem [*Legendre and Rassoulzadegan*, 1996]. With high NO$_3^-$ concentrations, large diatom blooms, and dominance by large krill and salps, fecal pellets and diatom aggregates were presumed to transport organic carbon to deep depths. Our results suggest that instead the WAP is a leaky ecosystem, in which low stratification both within and beneath the euphotic zone allow continual loss of particles by turbulent diffusion. High *f* ratios are thus balanced not by equally high *e* ratios but instead by a combination of vertical mixing that slowly transports suspended particles beneath the euphotic zone and moderate sinking flux. The depth horizon of remineralization of the vertically mixed material is thus likely to be substantially shallower than would be expected for sinking diatom aggregates or mesozooplankton fecal pellets, with correspondingly shorter sequestration times for the carbon transported out of the euphotic zone.

5. Conclusions

We used a suite of different methodologies to assess new, net community, and export production across both season-long temporal and region-wide spatial scales in the western Antarctic Peninsula. There was good agreement between measurements of new production (NO$_3^-$ drawdown and ^{15}NO$_3^-$ uptake) and NCP (O$_2$:Ar) and also good agreement between alternate methods of measuring export (sediment traps and ^{234}Th disequilibrium). However, new production was 5.3 times greater than export at our coastal site in the WAP, with new production measurements suggesting an efficient export ecosystem, and sinking flux measurements suggesting a recycling-dominated ecosystem. The imbalance between new and export production over the 144 days of our occupation of our coastal study site would equate to a difference ranging between 15 g N m^{-2} (new production) and 2.9 g N m^{-2} (export). If we considered our coastal region to be representative of the WAP at large and used Redfield C:N ratios to convert to carbon units, this would lead to a discrepancy in carbon export estimates of 18 Tg C over 5 months, as determined by *f* ratios versus *e* ratios.

To address this large imbalance we considered traditional nonsedimentation processes in the biological pump (including DOM export, diel vertical migration, and export mediated by higher trophic levels). However, the potential magnitudes of these processes were insufficient to close the budget. Instead, we suggest (based on a budget composed from NO$_3^-$, PN, and ^{234}Th vertical profiles) that transport of particles from the euphotic zone by vertical mixing may be equal to or greater than the flux of sinking particles. This alternate mechanism of vertical particle transport has important implications for carbon sequestration since vertically mixed particles will likely be remineralized at much shallower depths than rapidly sinking particles and vertical mixing will also transport CO$_2$ to the surface ocean from depth. Additionally, vertical mixing fluxes would also influence WAP plankton ecology as a significant loss term for phytoplankton.

Although no previous studies using multiple methods have been conducted across a sufficiently large spatial and long temporal scale to conclusively establish imbalances of new and export production in other

ecosystems, compelling evidence exists that new production exceeds export in many regions. Excess new production has been measured in the oligotrophic Sargasso Sea (f ratio = 0.39 and 0.08, e ratio = 0.04 and 0.06 for 1992 and 1993, respectively [*Lipschultz and Owens*, 1996; *Lomas et al.*, 2013]) with $^{15}NO_3^-$ uptake and sediment traps. In open ocean upwelling regions including the equatorial Pacific (f ratio = 0.14 and 0.26, ThE ratio < 0.10 [*Buesseler et al.*, 1995; *McCarthy et al.*, 1996; *Parker et al.*, 2011]) and Costa Rica upwelling Dome (f ratio~0.3, e ratio and ThE ratio~0.05 (Stukel, unpublished)) the ThE ratio (export/production determined by ^{234}Th) was significantly greater than the f ratio. Excess new production has also been found in the coastal California Current Ecosystem (f ratio = 0.2–0.8, NCP/C^{14}PP > 0.4, ThE ratio = 0.04–0.18, e ratio typically <0.2 [*Eppley et al.*, 1979; *Stukel et al.*, 2011; *Munro et al.*, 2013; *Stukel et al.*, 2013]) and Arabian Sea (f ratio = 0.17, ThE ratio = 0.075 [*Buesseler et al.*, 1998; *Sambrotto*, 2001]). A surplus of NCP relative to export was also found following an artificial Fe-enrichment experiment in the Subantarctic Atlantic open ocean [*Martin et al.*, 2013]. *Emerson* [2014] compiled annual NCP data from multiple models and satellite observations for comparison to export measurements in the oligotrophic Pacific, subarctic Pacific, and Sargasso Sea and found that export mediated by DOM and DVM by zooplankton may be enough to close the imbalance between sediment traps and NCP in the Pacific, but that total export in the Sargasso Sea is a factor of 3 less than NCP. Given the prevalence of this imbalance across such diverse ecosystems, it is reasonable to surmise that it may be a globally common phenomenon. If the leaky ecosystem concept applies to such other regions in which nitrate uptake is greater than export, we may need to reevaluate global estimates of the biological pump determined from sinking POC measurements.

References

Baker, E. T., H. B. Milburn, and D. A. Tennant (1988), Field assessment of sediment trap efficiency under varying flow conditions, *J. Mar. Res.*, 46, 573–592.

Benitez-Nelson, C. R., K. O. Buesseler, M. R. van der Loeff, J. Andrews, L. Ball, G. Crossin, and M. A. Charette (2001), Testing a new small-volume technique for determining Th-234 in seawater, *J. Radioanal. Nucl. Chem.*, 248, 795–799.

Bernard, K. S., and D. K. Steinberg (2013), Krill biomass and aggregation structure in relation to tidal cycle in a penguin foraging region off the western Antarctic Peninsula, *ICES J. Mar. Sci.*, 70, 834–849.

Buesseler, K., L. Ball, J. Andrews, C. Benitez-Nelson, R. Belastock, F. Chai, and Y. Chao (1998), Upper ocean export of particulate organic carbon in the Arabian Sea derived from thorium-234, *Deep Sea Res., Part II*, 45, 2461–2487.

Buesseler, K. O., J. A. Andrews, M. C. Hartman, R. Belastock, and F. Chai (1995), Regional estimates of the export flux of particulate organic carbon derived from thorium-234 during the JGOFS EqPac Program, *Deep Sea Res., Part II*, 42, 777–804.

Buesseler, K. O., J. E. Andrews, S. M. Pike, M. A. Charette, L. E. Goldson, M. A. Brzezinski, and V. P. Lance (2005), Particle export during the southern ocean iron experiment (SOFeX), *Limnol. Oceanogr.*, 50, 311–327.

Buesseler, K. O., et al. (2006), An assessment of particulate organic carbon to thorium-234 ratios in the ocean and their impact on the application of ^{234}Th as a POC flux proxy, *Mar. Chem.*, 100, 213–233.

Buesseler, K. O., et al. (2007), An assessment of the use of sediment traps for estimating upper ocean particle fluxes, *J. Mar. Res.*, 65, 345–416.

Buesseler, K. O., A. M. P. McDonnell, O. M. E. Schofield, D. K. Steinberg, and H. W. Ducklow (2010), High particle export over the continental shelf of the west Antarctic Peninsula, *Geophys. Res. Lett.*, 37, L22606, doi:10.1029/2010GL045448.

Carlson, C. A., H. W. Ducklow, D. A. Hansell, and W. O. Smith (1998), Organic carbon partitioning during spring phytoplankton blooms in the Ross Sea polynya and the Sargasso Sea, *Limnol. Oceanogr.*, 43, 375–386.

Clark, D. R., A. P. Rees, and I. Joint (2008), Ammonium regeneration and nitrification rates in the oligotrophic Atlantic Ocean: Implications for new production estimates, *Limnol. Oceanogr.*, 53, 52–62.

Conover, R. J. (1966), Assimilation of organic matter by zooplankton, *Limnol. Oceanogr.*, 11, 338–345.

Cowie, G. L., and J. I. Hedges (1996), Digestion and alteration of the biochemical constituents of a diatom (*Thalassiosira weissflogii*) ingested by an herbivorous zooplankton (*Calanus pacificus*), *Limnol. Oceanogr.*, 41, 581–594.

Craig, H., and T. Hayward (1987), Oxygen supersaturation in the ocean: Biological versus physical contributions, *Science*, 235, 199–202.

DiFiore, P. J., D. M. Sigman, and R. B. Dunbar (2009), Upper ocean nitrogen fluxes in the Polar Antarctic Zone: Constraints from the nitrogen and oxygen isotopes of nitrate, *Geochem. Geophys. Geosyst.*, 10, Q11016, doi:10.1029/2009GC002468.

Ducklow, H. W., and S. L. McCallister (2004), The biogeochemistry of carbon dioxide in the coastal oceans, in *The Global Coastal Ocean: Multiscale Interdisciplinary Processes*, edited by A. R. Robinson, K. Brink, and B. J. Rothschild, pp. 269–315, Harvard Univ. Press, Cambridge, Mass.

Ducklow, H. W., D. K. Steinberg, and K. O. Buesseler (2001), Upper ocean carbon export and the biological pump, *Oceanography*, 14, 50–58.

Ducklow, H. W., K. Baker, D. G. Martinson, L. B. Quetin, R. M. Ross, R. C. Smith, S. E. Stammerjohn, M. Vernet, and W. Fraser (2007), Marine pelagic ecosystems: The West Antarctic Peninsula, *Philos. Trans. R. Soc. London, Ser. B*, 362, 67–94.

Ducklow, H. W., M. Erickson, J. Kelly, M. Montes-Hugo, C. A. Ribic, R. C. Smith, S. E. Stammerjohn, and D. M. Karl (2008), Particle export from the upper ocean over the continental shelf of the west Antarctic Peninsula: A long-term record, 1992–2007, *Deep Sea Res., Part II*, 55, 2118–2131.

Ducklow, H. W., et al. (2013), West Antarctic Peninsula: An ice-dependent coastal marine ecosystem in transition, *Oceanography*, 26, 190–203.

Dugdale, R. C., and J. J. Goering (1967), Uptake of new and regenerated forms of nitrogen in primary productivity, *Limnol. Oceanogr.*, 12, 196–206.

Dugdale, R. C., and F. P. Wilkerson (1986), The use of N-15 to measure nitrogen uptake in eutrophic oceans: Experimental considerations, *Limnol. Oceanogr.*, 31, 673–689.

Emerson, S. (2014), Annual net community production and the biological carbon flux in the ocean, *Global Biogeochem. Cycles*, 28, 14–28, doi:10.1002/2013GB004680.

Eppley, R. W., and B. J. Peterson (1979), Particulate organic matter flux and planktonic new production in the deep ocean, *Nature*, 282, 677–680.

Eppley, R. W., E. H. Renger, and W. G. Harrison (1979), Nitrate and phytoplankton production in southern California coastal waters, *Limnol. Oceanogr.*, *24*, 483–494.

Gardner, W. D., I. D. Walsh, and M. J. Richardson (1993), Biophysical forcing of particle production and distribution during a spring bloom in the North Atlantic, *Deep Sea Res., Part II*, *40*, 171–195.

Gardner, W. D., S. P. Chung, M. J. Richardson, and I. D. Walsh (1995), The oceanic mixed-layer pump, *Deep Sea Res., Part II*, *42*, 757–765.

Garrett, C., and W. Munk (1972), Oceanic mixing by breaking internal waves, *Deep Sea Res.*, *19*, 823–832.

Grundle, D. S., S. K. Juniper, and K. E. Giesbrecht (2013), Euphotic zone nitrification in the NE subarctic Pacific: Implications for measurements of new production, *Mar. Chem.*, *155*, 113–123.

Hannides, C. C. S., M. R. Landry, C. R. Benitez-Nelson, R. M. Styles, J. P. Montoya, and D. M. Karl (2009), Export stoichiometry and migrant-mediated flux of phosphorus in the North Pacific Subtropical Gyre, *Deep Sea Res., Part I*, *56*, 73–88.

Hansell, D. A., and C. A. Carlson (Eds.) (2002), *Biogeochemistry of Marine Dissolved Organic Matter*, Elsevier Science, San Diego, Calif.

Hedges, J. I. (1992), Global biogeochemical cycles: Progress and problems, *Mar. Chem.*, *39*, 67–93.

Helly, J. J., R. S. Kaufmann, G. R. Stephenson, and M. Vernet (2011), Cooling, dilution and mixing of ocean water by free-drifting icebergs in the Weddell Sea, *Deep Sea Res., Part II*, *58*, 1346–1363.

Huang, K., H. W. Ducklow, M. C. Vernet, N. Cassar, and M. M. Bender (2010), Export production and its regulating factors in the West Antarctica Peninsula region of the Southern Ocean, *Global Biogeochem. Cycles*, *26*, GB2005, doi:10.1029/2010GB0040.

Isaaks, E. H., and R. Sarivasta (1989), *An Introduction to Applied Geostatistics*, Oxford Univ. Press, Oxford, U. K.

Kato, M., S. Segawa, E. Tanoue, and M. Murano (1982), Filtering and ingestion rates of the Antarctic krill, *Euphausia Superba Dana*, *Trans. Tokyo Univ. Fish.*, *5*, 167–175.

Klinck, J. M., E. E. Hofmann, R. C. Beardsley, B. Salihoglu, and S. Howard (2004), Water-mass properties and circulation on the west Antarctic Peninsula Continental Shelf in Austral Fall and Winter 2001, *Deep Sea Res., Part II*, *51*, 1925–1946.

Knauer, G. A., J. H. Martin, and K. W. Bruland (1979), Fluxes of particulate carbon, nitrogen, and phosphorus in the upper water column of the Northeast Pacific, *Deep Sea Res. Part A*, *26*, 97–108.

Knox, G. A. (2006), *Biology of the Southern Ocean*, CRC Press, Boca Raton, Fla.

Krige, D. G. (1951), A statistical approach to some basic mine valuation problems on the witwatersrand, *J. Chem. Metall. Min. Soc. South Africa*, *52*, 119–139.

Legendre, L., and F. Rassoulzadegan (1996), Food-web mediated export of biogenic carbon in oceans: Hydrodynamic control, *Mar. Ecol. Prog. Ser.*, *145*, 179–193.

Lipschultz, F., and N. J. P. Owens (1996), An assessment of nitrogen fixation as a source of nitrogen to the North Atlantic Ocean, *Biogeochemistry*, *35*, 261–274.

Lomas, M. W., N. R. Bates, R. J. Johnson, A. H. Knap, D. K. Steinberg, and C. A. Carlson (2013), Two decades and counting: 24-years of sustained open ocean biogeochemical measurements in the Sargasso Sea, *Deep Sea Res., Part II*, *93*, 16–32.

Martin, P., et al. (2013), Iron fertilization enhanced net community production but not downward particle flux during the Southern Ocean iron fertilization experiment LOHAFEX, *Global Biogeochem. Cycles*, *27*, 871–881, doi:10.1002/gbc.20077.

Martinson, D. G., S. E. Stammerjohn, R. A. Iannuzzi, R. C. Smith, and M. Vernet (2008), Western Antarctic Peninsula physical oceanography and spatio-temporal variability, *Deep Sea Res., Part II*, *55*, 1964–1987.

McCarthy, J. J., C. Garside, J. L. Nevins, and R. T. Barber (1996), New production along 140°W in the equatorial Pacific during and following the 1992 El Niño event, *Deep Sea Res., Part II*, *43*, 1065–1093.

Michaels, A. F., and M. W. Silver (1988), Primary production, sinking fluxes and the microbial food web, *Deep Sea Res. Part A*, *35*, 473–490.

Moline, M. A., O. Schofield, and N. P. Boucher (1998), Photosynthetic parameters and empirical modelling of primary production: A case study on the Antarctic Peninsula shelf, *Antarct. Sci.*, *10*, 45–54.

Montes-Hugo, M., S. C. Doney, H. W. Ducklow, W. Fraser, D. Martinson, S. E. Stammerjohn, and O. Schofield (2009), Recent changes in phytoplankton communities associated with rapid regional climate change along the western Antarctic Peninsula, *Science*, *323*, 1470–1473.

Munro, D. R., P. D. Quay, L. W. Juranek, and R. Goericke (2013), Biological production rates off the Southern California coast estimated from triple O_2 isotopes and O_2:Ar gas ratios, *Limnol. Oceanogr.*, *58*, 1312–1328.

Newell, S. E., S. E. Fawcett, and B. B. Ward (2013), Depth distribution of ammonia oxidation rates and ammonia-oxidizer community composition in the Sargasso Sea, *Limnol. Oceanogr.*, *58*, 1491–1500.

Olivieri, R. A., and F. P. Chavez (2000), A model of plankton dynamics for the coastal upwelling system of Monterey Bay, California, *Deep Sea Res., Part II*, *47*, 1077–1106.

Olson, R. J. (1981), Differential photoinhibition of marine nitrifying bacteria: A possible mechanism for the formation of the primary nitrate maximum, *J. Mar. Res.*, *39*, 227–238.

Owens, S. A. (2013), Advances in measurements of particle cycling and fluxes in the ocean.

Owens, S. A., K. O. Buesseler, and K. W. W. Sims (2011), Re-evaluating the [238]U-salinity relationship in seawater: Implications for the [238]U-[234]Th disequilibrium method, *Mar. Chem.*, *127*, 31–39.

Parker, A. E., F. P. Wilkerson, R. C. Dugdale, A. Marchi, and V. Hogue (2011), Patterns of nitrogen concentration and uptake by two phytoplankton size-classes in the equatorial Pacific Ocean (110°W - 140°W) during 2004 and 2005, *Deep Sea Res., Part II*, *58*, 417–433.

Passow, U., J. Dunne, J. W. Murray, L. Balistrieri, and A. L. Alldredge (2006), Organic carbon to Th-234 ratios of marine organic matter, *Mar. Chem.*, *100*, 323–336.

Pesant, S., L. Legendre, M. Gosselin, E. Bauerfeind, and G. Budeus (2002), Wind-triggered events of phytoplankton downward flux in the Northeast Water Polynya, *J. Mar. Syst.*, *31*, 261–278.

Pike, S. M., K. O. Buesseler, J. Andrews, and N. Savoye (2005), Quantification of [234]Th recovery in small volume sea water samples by inductively coupled plasma-mass spectrometry, *J. Radioanal. Nucl. Chem.*, *263*, 355–360.

Plattner, G. K., N. Gruber, H. Frenzel, and J. C. McWilliams (2005), Decoupling marine export production from new production, *Geophys. Res. Lett.*, *32*, L11612, doi:10.1029/2005GL022660.

Reuer, M. K., B. A. Barnett, M. L. Bender, P. G. Falkowski, and M. B. Hendricks (2007), New estimates of Southern Ocean biological production rates from O-2/Ar ratios and the triple isotope composition of O-2, *Deep Sea Res., Part I*, *54*, 951–974.

Sambrotto, R. N. (2001), Nitrogen production in the northern Arabian Sea during the Spring Intermonsoon and Southwest Monsoon seasons, *Deep Sea Res., Part II*, *48*, 1173–1198.

Savoye, N., C. Benitez-Nelson, A. B. Burd, J. K. Cochran, M. Charette, K. O. Buesseler, G. A. Jackson, M. Roy-Barman, S. Schmidt, and M. Elskens (2006), [234]Th sorption and export models in the water column: A review, *Mar. Chem.*, *100*, 234–249.

Smith, D. A., and J. M. Klinck (2002), Water properties on the west Antarctic Peninsula continental shelf: A model study of effects of surface fluxes and sea ice, *Deep Sea Res., Part II*, *49*, 4863–4886.

Smith, K. L., A. D. Sherman, T. J. Shaw, and J. Sprintall (2013), Icebergs as unique Lagrangian ecosystems in polar seas, *Annu. Rev. Mar. Sci.*, *5*(5), 269–287.

Smith, R. C., K. S. Baker, H. M. Dierssen, S. E. Stammerjohn, and M. Vernet (2001), Variability of primary production in an Antarctic marine ecosystem as estimated using a multi-scale sampling strategy, *Am. Zool.*, *41*, 40–56.

Stein, M. L. (1999), *Interpolation of Spatial Data: Some Theory for Kriging*, Springer, New York.

Steinberg, D. K., C. A. Carlson, N. R. Bates, S. A. Goldthwait, L. P. Madin, and A. F. Michaels (2000), Zooplankton vertical migration and the active transport of dissolved organic and inorganic carbon in the Sargasso Sea, *Deep Sea Res., Part I*, *47*, 137–158.

Steinberg, D. K., D. G. Martinson, and D. P. Costa (2012), Two decades of pelagic ecology of the western Antarctic Peninsula, *Oceanography*, *25*, 56–67.

Straile, D. (1997), Gross growth efficiencies of protozoan and metazoan zooplankton and their dependence on food concentration, predator–prey weight ratio, and taxonomic group, *Limnol. Oceanogr.*, *42*, 1375–1385.

Strickland, J. D., and T. R. Parsons (1972), *A Practical Handbook of Seawater Analysis*, vol. 167, 2nd ed., Bulletin of the Fisheries Research Board of Canada, Ottawa.

Stukel, M. R., M. R. Landry, C. R. Benitez-Nelson, and R. Goericke (2011), Trophic cycling and carbon export relationships in the California Current Ecosystem, *Limnol. Oceanogr.*, *56*, 1866–1878.

Stukel, M. R., M. D. Ohman, C. R. Benitez-Nelson, and M. R. Landry (2013), Contributions of mesozooplankton to vertical carbon export in a coastal upwelling system, *Mar. Ecol. Prog. Ser.*, *491*, 47–65.

Tortell, P. D., E. C. Asher, H. W. Ducklow, J. A. L. Goldman, J. W. H. Dacey, J. J. Grzymski, J. N. Young, S. A. Kranz, K. S. Bernard, and F. M. M. Morel (2014), Metabolic balance of coastal Antarctic waters revealed by autonomous pCO_2 and $\Delta O_2/Ar$ measurements, *Geophys. Res. Lett.*, *41*, 6803–6810, doi:10.1002/2014GL061266.

Waniek, J. J. (2003), The role of physical forcing in initiation of spring blooms in the northeast Atlantic, *J. Mar. Syst.*, *39*, 57–82.

Waples, J. T., C. Benitez-Nelson, N. Savoye, M. R. Van der Loeff, M. Baskaran, and O. Gustafsson (2006), An introduction to the application and future use of [234]Th in aquatic systems, *Mar. Chem.*, *100*, 166–189.

Ward, B. B., R. J. Olson, and M. J. Perry (1982), Microbial nitrification rates in the primary nitrite maximum off Southern California, *Deep Sea Res.*, *29*, 247–255.

Yool, A., A. P. Martin, C. Fernandez, and D. R. Clark (2007), The significance of nitrification for oceanic new production, *Nature*, *447*, 999–1002.

Young, J. N., J. A. L. Goldman, S. A. Kranz, P. D. Tortell, and F. M. M. Morel (2014), Slow carboxylation of Rubisco constrains the rate of carbon fixation during Antarctic phytoplankton blooms, *New Phytol.*, *205*, 172–181.